OXIDATIVE DISSOLUTION OF PYRITE:
A COMBINED EXPERIMENTAL AND IRON ISOTOPE INVESTIGATION

by

AMY LYNN WOLFE

B.S. Marine Science, University of South Carolina, 2001

Submitted to the Graduate Faculty of

Arts and Sciences in partial fulfillment

of the requirements for the degree of

Doctor of Philosophy

University of Pittsburgh

2010

UNIVERSITY OF PITTSBURGH

FACULTY OF ARTS AND SCIENCES

This dissertation was presented

by

Amy Lynn Wolfe

It was defended on

November 5, 2010

and approved by

Dr. Thomas H. Anderson, Professor, University of Pittsburgh

Dr. Daniel Bain, Assistant Professor, University of Pittsburgh

Dr. Rosemary Capo, Associate Professor, University of Pittsburgh

Dr. David A. Dzombak, Professor, Carnegie Mellon University

Dr. Michael Rosenmeier, Assistant Professor, University of Pittsburgh

Dissertation Advisor: Dr. Brian Stewart, Associate Professor, University of Pittsburgh

OXIDATIVE DISSOLUTION OF PYRITE:
A COMBINED EXPERIMENTAL AND IRON ISOTOPE INVESTIGATION

Amy Wolfe, PhD

University of Pittsburgh, 2010

This work focuses on the geochemistry and iron isotope systematics of pyrite from hydrothermal and coal-forming environments. Dissolution of pyrite, even under abiotic conditions, is difficult to study experimentally and previous studies have demonstrated that the rate of pyrite oxidation is dependent upon environmental conditions. Knowledge of dissolution mechanisms enables more accurate reaction rate measurements, and will improve the ability to predict the temporal changes in chemistry of ground and surface waters that come into contact with pyrite.

The first aspect of the research presented here focuses on the need for standardization of sample preparation techniques to allow for experimental and interlaboratory comparison of pyrite dissolution experiments. A reproducible sample preparation technique for pyrite that yields clean, uniform grains within a narrow size range of interest was developed. It was shown that use of this method in pyrite dissolution experiments significantly reduces artifacts related to unconstrained surface area exposure to fluids.

In the second portion of this work, iron isotopes were analyzed to quantify and source-track the dissolution of pyrite during abiotic pyrite dissolution experiments performed on hydrothermal and sedimentary pyrites. The hydrothermal pyrite δ^{56}Fe values fall within the range of previously measured values, but the coal/sedimentary values are higher than those previously measured for any Phanerozoic sedimentary pyrite. Leachates from oxidative dissolution of the

pyrite at pH=3 tend, with minor exceptions, to yield $\delta^{56}Fe$ values equal to or below those of the coexisting bulk pyrite, by up to ~1‰. This is generally consistent with theoretical fractionation calculations. Iron isotopes could be a useful tool in distinguishing between waters that interact with coal-derived pyrite and pyrite formed under marine conditions.

The third section focuses on extracting sedimentary pyrite and other minerals under typical near-surface temperatures and environments, which is complicated by the small grain size and complex nature of the phases found in the sedimentary environment. An extraction method was developed to better characterize the nature of iron behavior between phases present in coal forming environments. A proposed iron extraction method and testing procedure is outlined for future studies of Fe speciation in coal.

TABLE OF CONTENTS

LIST OF TABLES

LIST OF FIGURES

PREFACE

This work is dedicated to:

Ainslee Grace Aycock, Julia Eden Chapman, and Jack Teschke:

the next generation of scientists.

And

To RR:

I cannot begin to thank you enough for your professionalism, objectivity, and advice. Thank you for supporting me, believing in me, and appreciating me for who I am.

****

This research was funded, in part, by the National Science Foundation under grant EAR-0228903 and EAR-0229019. I would like to thank the NSF GK-12 Fellowship Program and University of Pittsburgh A.W. Mellon Fellowship for providing partial financial support for two years of graduate school.

To Drs. Brian Stewart and Rosemary Capo: thank you for your patience, encouragement, and financial support...for introducing me to the finer aspects of science research and writing, keeping me on track, and for teaching/showing me (or at least trying to) when to stop – science is never (really) finished.

The intellectual content and quality of this dissertation were greatly improved by the members of my doctorate committee, and former grad student Dr. Ran Liu. I am grateful for your input, mentorship and expert contributions as coauthors.

To Dr. Tom Anderson – your objectivity, humor, advice, kindness and encouragement are deeply appreciated. Thank you for believing in me.

I am grateful for the patience and insight extended to me by Dr. Dan Bain. Many thanks for taking time to answer all of my chemistry questions, and listen to my ideas and hypotheses regarding topics other than my research. I am grateful for your support and encouragement.

A special thank you is extended to Dr. Ian Butler (University of Edinburgh), Dr. Stephen Grimes (University of Plymouth), Dr. James Hower (University of KY), and Jay Winter for providing their time, as well as coal and pyrite samples for experimental work. Much appreciation is extended to Ian Butler, Dr. Hower, and Dr. Zondlo for their geochemical insight, wisdom, and encouragement regarding my research.

I also thank the Department of Geology and Planetary Science, University of Pittsburgh, for the opportunity to conduct my graduate research, teach, and be financial supported for numerous semesters as a teaching assistant, as well as their technical and administrative support. Specifically in Geology's main office, thanks to Matt Romick, Deanna Hitchcock, Dolly Chavez, Lorraine Robbins and Shannon Granahan for all their logistical support. Shannon deserves a special award for weathering with me – and always with a smile - the innumerous bizarre administrative situations I have experienced as a graduate student.

Many thanks to Dr. Charlie Jones and Dr. Ian Skilling for arranging summer financial support and putting me to work – I doubt I will ever forget the many hours spent in the basement organizing rocks and minerals.

To my fellow Geochem lab mates, past and present (Tonya Brubaker, Liz Chapman, James Gardiner, Justin Hynicka, Lev Spivak-Birndorf): pizza, powerpoints, ICP maintenance, bottle washing, and the Sierras. Many of my fondest memories of graduate school will include you.

I cannot forget the many friendships I have shared with officemates. Topher: I appreciate your ability to make bad puns and find humor in all things. And Damian – Moxie, "your mom", weird food, weekends spent at school, coffee breaks, and laughing until we cried. School was way too much fun! I am grateful and humbled by your friendship, advice, loyalty, and unbiased support.

To my mineralogy students: Aaron P., Alex D., Anna S., Brianna S., Bryan T., Chelsea D., Ellen F., Everett R., James U., Jess M., Jill B., Jim T., Kat W., Kelly F., Lucy R., Maria P., Maria S., Mary Kate E., Mike W., Nick H., Peter B., Shawn C., and Tama T. It has been a crazy semester - and a bumpy ride - and I am privileged to have taught you. Many thanks for your patience, humor, and challenging questions. It has been wonderful getting to know you and I wish you all the best! I am confident that each of you will go far.

Erin (my conscience): I am thankful for all of the assistance you provided this semester. Your no-nonsense attitude, forthright honesty, encouragement and support was/is deeply appreciated. Three cheers to our table at Fuel and Fuddle, tomatoes, time management, and goofy conversations. Thank you for being there.

Tamara, Katie and Liz: Thank you for showing me the true meaning of friendship; for giving objective advice, letting me know when I was wrong, laughing when I goofed, and listening when life

dealt a crazy hand. Liz – I will always remember to (try) to be slow to anger, slow to speak but quick to listen and make merchandise returns. I love you all.

Stephen: between the two of us, we have seen each other through four degrees, two states, one country and 10+ years of friendship. I don't think I have laughed or cried with anyone as much as you. I have learned much about myself through our friendship. Thank you for looking out for me, caring, for unsolicited (but always appreciated) advice, for believing in me and picking me up when I fell down. I maintain, with strong conviction, that we were siblings in another lifetime and I love you dearly. PS. Please return my goats.

For your love, support, understanding, and advice: Mom, Dad, Grandma, Pappa, Judy and Les. I could not have made the journey without you. Mom-thank you for teaching me to be resourceful and to use what I have: I attribute my passion for methodology development and "out-of-the-box" thinking to you. I appreciate everything you have done and know that, at times, you sacrificed your own wishes and goals so Kim and I could achieve ours. Dad – you taught me that I should let no one can tell me what I can or can't do – and this resonates in my mind as I finish my tenure as a graduate student. To my grandparents: your unfailing encouragement and support have been a great source of comfort. I cannot begin to thank you for the values you have instilled within me or the sacrifices you made for our family. I have been lucky enough to have a second set of parents: Judy and Les, I am humbled by your kindness and love. Thank you for bringing me into your family.

And to Kimmy, my sister and best friend. You are the silliest, goofiest person I know. I can always count on you to make me laugh. You have the biggest heart of anyone I have ever met and the world would be a better place if there were more people like you. Thanks for taking care of me even though we were separated by hundreds of mile. And mostly, thanks for seeing me through.

1.0 INTRODUCTION

Iron sulfides constitute a diverse group of solid and dissolved complexes within aquatic systems. Pyrite (FeS_2), the most common sulfide mineral in Earth's surface environments, is found in a wide variety of geologic environments. Pyrite can form under high temperature conditions, including contact metamorphism and hydrothermal fluid circulation, as well as in low temperature (<100°C) sedimentary environments. In sedimentary environments, pyrite is a redox buffer under anoxic conditions and its presence is a strong indicator of reducing conditions (Descostes et al., 2004). Sulfides are essential in regulating and controlling global geochemical iron and sulfur cycles. Sulfides also demonstrate significant complexity within low temperature environments in which a number of metastable phases become significant in biogeochemical processes (Rickard and Luther, 2007).

Pyrite dissolution that leads to acidification of water releases high concentrations of iron, sulfuric acid, and other potentially harmful metals. Iron and related metals are mobile and bioavailable, and may rise to toxic levels within the environment Acid mine drainage (AMD) (Younger, 2002), a product of pyrite dissolution, is generated through a series of linked complex geochemical- and microbial–mediated reactions that occur when water comes in contact with coal and confining rocks, such as shale, containing pyrite. AMD continues to be the most serious water quality and watershed degradation issue for coal-mining areas in the Appalachian and Rocky Mountains and metal-mining regions of the western United States.

A generic term “acid sulfate soil” (CLASS) is used to describe a similar process that occurs in coastal, commonly hydromorphic Holocene sediments containing pyrite (Collins and Waite, 2009). The presence of Fe, derived from CLASS, in coastal environments has been implicated in stimulating harmful algal blooms that may play a critical role in massive fish kills caused by low levels of dissolved oxygen (Collins and Waite, 2009). In both AMD and CLASS outflows, the source from which iron is being transported is not well constrained.

In order to effectively address the negative issues associated with the presence of Fe-enriched water, the processes and mechanisms governing pyrite dissolution and the subsequent geochemical evolution of water need to be understood. Most experimental studies of pyrite dissolution are conducted with hydrothermal pyrite. These show that the rate of pyrite oxidation is dependent upon factors such as pH, dissolved oxygen, ferric iron concentration and the presence of iron- or sulfur-oxidizing bacteria. Estimated rates of oxidation in field systems commonly differ substantially, probably because dissolution of sedimentary pyrite present in natural systems is accelerated in the presence of bacteria.

Development of new methods to study dissolution of sedimentary pyrite is a principal goal of this dissertation. Knowledge of dissolution mechanisms enables more accurate reaction rate measurements, and will improve the ability to predict the temporal changes in chemistry of ground and surface waters that come into contact with pyrite. Methods commonly used to characterize and provide insight into geochemical products and processes at the Earth’s surface typically involve analyses of the stable isotopes of hydrogen, carbon, oxygen and sulfur. Distinct isotopic ratios in water may be determined by source and the evaporation-precipitation history. Innovative developments in mass spectrometry now provide scientists opportunities to explore

transition metal isotope systems, such as iron (Anbar et al., 2000; Beard and Johnson, 1999; Brantley et al., 2001; Johnson and Beard, 1999).

In this study, iron isotopes are employed to characterize the dissolution of pyrite and identify sources from which AMD are derived. Iron, an essential, redox-sensitive element, has four naturally occurring isotopes: ^{54}Fe, ^{56}Fe, ^{57}Fe, and ^{58}Fe. The mass difference between isotope pairs is sufficient to lead to measurable mass fractionation during low temperature processes (Polyakov, 1997; Schauble et al., 2001; Urey, 1947). ^{58}Fe abundances are extremely small (0.28%) so isotopic variations are described using ^{54}Fe (5.9%), ^{56}Fe (91.72%) and ^{57}Fe (2.1%) ratios. Isotopic data are reported using the δ notation relative to the international Fe standard IRMM-14 which is a synthetic standard supplied as metallic Fe (Duan et al., 2010):

$$\delta^{56}Fe = \left(\frac{{}^{56}Fe/{}^{54}Fe_{sample}}{{}^{56}Fe/{}^{54}Fe_{IRMM}} - 1\right) \times 1000$$

The processes of iron mobilization and mass transfer contribute to iron-isotope fractionation in low-temperature geological settings. Isotopes of iron are fractionated during biogenic and inorganic redox processes, complexation with soil organic matter, bacterial interactions, and during surface adsorption and mineral precipitation reactions ((Borrok et al., 2008) and references therein). Iron isotopes have been used as a tool to examine source and mechanisms of controlling Fe-cycling in freshwater environments and soils (Bergquist and Boyle, 2006; Borrok et al., 2008; Emmanuel et al., 2005; Fantle and DePaolo, 2005; Ingri et al., 2006) and more recently, during oxidative weathering of sulfide-rich rocks and minerals (Borrok et al., 2008; Fernandez and Borrok, 2009; Herbert and Schippers, 2008). Analyses of iron isotopes in pyrite have largely yielded depleted δ^{56}Fe values, with a range of 0.5 to -3.5‰ (Fehr et al., 2010; Matthews et al., 2004; Rouxel et al., 2005; Severmann et al., 2006; Yamaguchi et al., 2007).

Samples for these studies were collected mainly from modern and ancient marine environments. Pyrite formation in modern organic-rich environments is mediated by sulfate-reducing bacteria and proceeds through the dissolution of lithogenic iron oxides (Rouxel et al., 2005); organic matter acts as a reducing agent for sulfate as well as an energy source for bacterial activities. Depleted isotopic signatures suggest that fractionation is dominated by biogenic reduction of Fe(III) oxides (see above references). The current assumption is that diagenetic pyrite is a passive recorder of the Fe isotope composition of a reduced Fe reservoir in which the heavier isotopes are removed through the precipitation of iron oxides, but no experimental data exist to support this hypothesis (Butler et al., 2005). Theoretical estimates using Mössbauer and vibrational spectroscopy indicated significant fractionation effects occurring between pyrite and ferrous iron (Polyakov and Mineev, 1999; Schauble et al., 2001); however, interpretations remain somewhat unclear given the lack of experimental determination of Fe fractionation factors associated with pyrite formation and dissolution (Severmann et al., 2006).

In this study, iron isotopes are used to study dissolution rates of different pyrite types (hydrothermal versus sedimentary). This is the first investigation of iron isotope fractionation occurring during pyrite oxidation. Data from this work demonstrates the complexity of modeling fractionation between FeS_2*(s)* and Fe(II)(*aq)* when natural pyrite samples are used, as opposed to theoretical calculations (Domagal-Goldman and Kubicki, 2008; Polyakov and Mineev, 1999; Schauble et al., 2001).

Further, the relationship between sedimentary pyrite dissolution and the geochemical evolution of water is examined. Analysis of pyrite collected from coal seams, and modern peat analogs, may provide important constraints on the mechanisms and pathways, biological and inorganic, involved in producing Fe isotope variations during pyrite formation (**Fig. 1**). Pyrite

formation in ancient peat environments, now preserved as coal, reflect formation under conditions unlike those persisting in most marine, brackish and freshwater environments. Based on these results, iron isotope are used: 1) to provide a framework for the interpretation and calibration of isotopic compositions measured during pyrite dissolution, 2) to assess the efficacy of pyrite as a geochemical tracer and, 3) to reveal the role of pyrite in paleoredox studies.

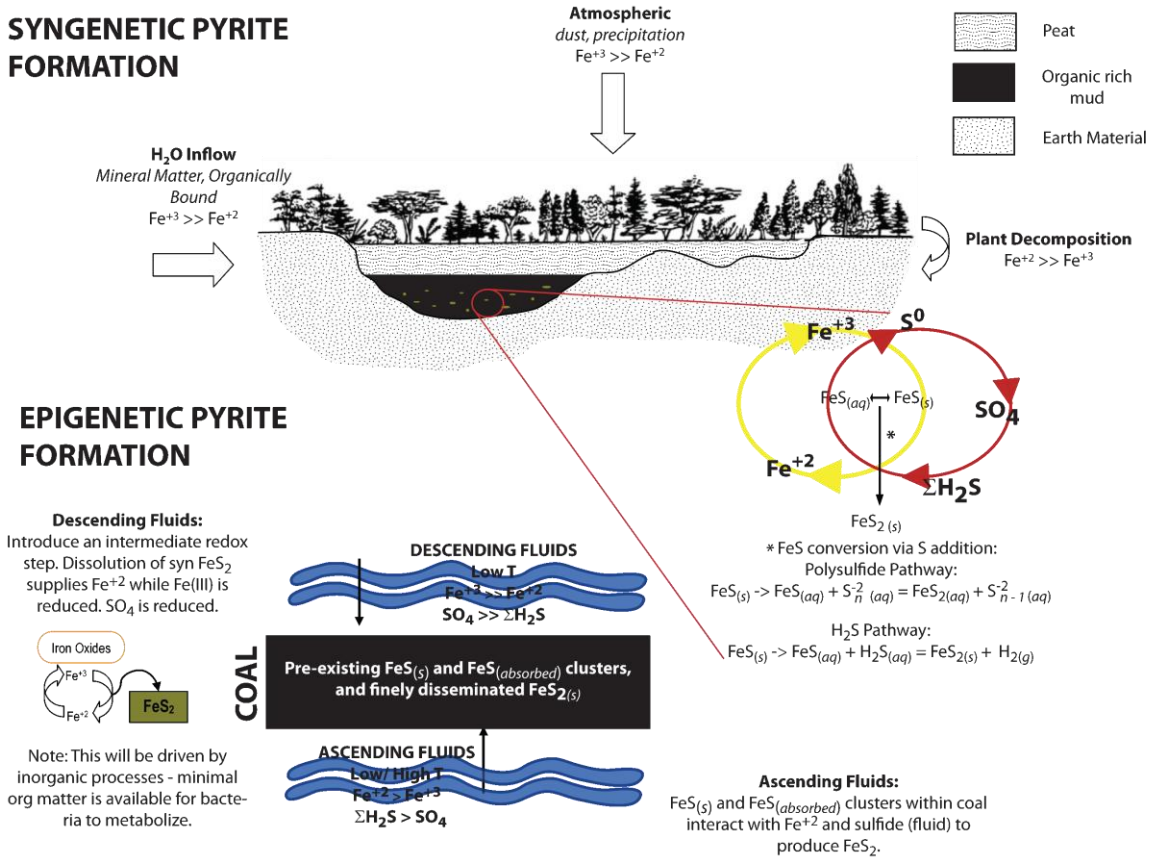

Figure 1. The nature of pyrite formation in ancient peat mires and within coal.

1.1.1 Research Objectives

The ubiquity of iron in AMD outflows, in conjunction with its tendency to participate in geochemical and biogeochemical reactions, suggests that there is great potential for finding significant, and therefore useful, variations in Fe isotope compositions that record the

fractionation associated with the reactions. Analyses of changes that occur during oxidative pyrite dissolution improves our understanding of iron movement within Fe-bearing outflows, and provides insight into the biogeochemistry of this element, reaction mechanisms and processes that occur in solid-liquid systems.

The objectives of this research are to:

1. Develop methods that allow reproducible experimental results on naturally-occurring pyrite.
2. Determine the $^{56}Fe/^{54}Fe$ variation of hydrothermal pyrite and sedimentary pyrite deposited under different environmental conditions.
3. Establish if abiotic pyrite dissolution causes measurable shifts in the $^{56}Fe/^{54}Fe$ ratio of iron released into solution.
4. Evaluate the use of iron isotopes as tracers for the primary source of iron in contaminated outflows.
5. Determine the partitioning of iron among different phases in organic-rich sediments such as coal, and its relationship to pyrite petrogenesis.

1.1.2 Dissertation Overview

The usefulness of iron isotopes in the study of abiotic pyrite dissolution is presented in five chapters. Chapters 2, 3 and 4 comprise the core of the dissertation. The results presented in Chapter 2, "*A method for generating uniform size-segregated pyrite particle fractions*" is a published manuscript in a peer-review journal, Geochemical Transactions (Wolfe et al., 2007). The paper is co-authored by Dr. Ran Liu, Dr. David Dzombak, Dr. Brian Stewart and Dr. Rosemary Capo. This work was part of a comparative investigation of dissolution rates for pyrite

from different petrogenetic environments; the objective was to assess dry and wet sieving preparation methodologies, and to develop a reproducible technique that yielded uniformly size-distributed material within a limited size range of interest. The article describes a wet sieving preparation method that successfully concentrates pyrite particles within a 44–75 μm diameter range. Experimental results demonstrate that there is a need to standardize sample preparation techniques to allow accurate comparisons of pyrite dissolution experiments under diverse conditions.

Results obtained from iron isotope analyses of experimental abiotic pyrite dissolution experiments are presented in Chapter 3, *Oxidative Dissolution of Pyrite: A Combined Experimental and Iron Isotope Investigation*. This research demonstrates that pyrite from different geologic environments a) exhibits unique dissolution behavior, b) bears distinct isotopic signatures, and c) generates depleted δ^{56}Fe pools during pyrite oxidation. Part of the work, conducted in collaboration with Dr. Ran Liu and Dr. David Dzombak at Carnegie Mellon University, that addresses pyrite dissolution kinetics using experimental and electrochemical techniques have been incorporated into three publications. I am second author in each publication.

The results presented in Chapter 4, entitled "*Partitioning of iron in organic and mineral phases: sequential extractions of bituminous coal*," are part of an investigation of pyrite formation in organic-rich sediments, including coal. A sequential extraction method was developed that yields detailed information on the speciation of iron in coal. Six sediment iron fractions are characterized (1) surficially bonded Fe; (2) organically bound Fe (Fe_{org}); (3) carbonate-associated Fe, including siderite and ankerite; (4) reducible oxides, including ferrihydrite, lepidocrocite, goethite; (5) silicate Fe; and (6) pyrite Fe. Iron fractions were

determined using a combination of pressurized fluid extraction, using EDTA and NMP, as well as acid leaching on a suite of bituminous coal samples collected from different coal regions within Pennsylvania. Data reveal that >90% of iron is surficially bound, and easily removed using EDTA. The chemical leach designed to extract iron was marginally successful.

Chapter 5 summarizes the original contributions, major findings and conclusions from this work and provides suggestions for future work using iron isotopes to investigate 1) pyrite formation; 2) pyrite dissolution and 3) application as a geochemical tracer in contaminated outflows.

2.0 A METHOD FOR GENERATING UNIFORM SIZE-SEGREGATED PYRITE PARTICLE FRACTIONS

2.1 BACKGROUND

Pyrite, $FeS_{2,}$ is one of the most abundant sulfide minerals at the Earth's surface and represents an important reservoir for iron and sulfur within the Earth's crust. It exists in a variety of forms and is prevalent in numerous environments including hydrothermal ore zones, modern lake and ocean sediments, and sedimentary rocks. Regardless of its source, the weathering of pyrite via oxidative dissolution can result in the acidification and degradation of water resources (Evangelou, 1995; Kamei and Ohmoto, 2000; Lowson, 1982; Moses et al., 1987; Rigby et al., 2006; Rimstidt and Vaughan, 2003; Weber et al., 2004; Williamson and Rimstidt, 1994) and references therein). The rates and mechanisms governing this process are only partially understood despite numerous experimental studies of pyrite oxidation (Bonnissel-Gissinger et al., 1998; Caldeira et al., 2003; Cruz et al., 2001; Descostes et al., 2004; Jerz and Rimstidt, 2004; Liu, 2006; McGuire et al., 2001; McKibben and Barnes, 1986; Paschka, 2004).

In pyrite dissolution and oxidation experiments, massive hydrothermal pyrite is normally used because it is readily available and well characterized. However, sedimentary pyrite exists in many forms, and pyrite mineral preparation methodologies are inconsistent within the literature (Table 1). Previous research (Bonnissel-Gissinger et al., 1998; McKibben and Barnes, 1986)

indicates that differences in grain size (i.e., surface area) can exert significant control on pyrite oxidation rates, and, in general, there is a positive, linear correlation between surface area and the rate of pyrite oxidation (Hammack RW, 1988). Pyrite powders are usually prepared by grinding a homogenous, massive pyrite sample using an agate mortar and pestle (Caldeira et al., 2003; Cruz et al., 2001; Kamei and Ohmoto, 2000; McGuire et al., 2001) or a mixer mill (Sasaki, 1994). To achieve a specific size range of material for experiments, samples are either dry sieved (Caldeira et al., 2003; McGuire et al., 2001), wet sieved (Cruz et al., 2001), or both (Rimstidt and Vaughan, 2003). Sieved samples are then cleaned in various ways to remove fine particles adhering to the mineral surface and oxidation products prior to use.

The objective of this work was to develop an effective, reproducible procedure for isolating pyrite grains in the 44-75 μm range for dissolution studies. This work was conducted as part of a comparative investigation of dissolution rates for pyrite from different petrogenetic environments. Previous pyrite dissolution experiments (**Table 1**) involved hydrothermal pyrite particles >75 μm in diameter, while our experiments called for a smaller size fraction, 44-75 μm, to better simulate dissolution of finely disseminated pyrite in some sedimentary environments. We compared dry and wet sieving preparation methodologies with the goal of developing a reproducible technique that yields clean material within our size range of interest. The methods were evaluated through a combination of SEM analysis and batch dissolution experiments.

Table 1. Pyrite preparation methodologies used in previous studies. In each method listed, the pyrite was hydrothermal in origin.

Target Size Fraction (μm)	Methodology	Reference
125 – 250 μm	The pyrite was crushed, soaked overnight in hot hydrofluoric acid, washed in distilled water, dried in air and sieved. Sieved pyrite was ultrasonically cleaned in ethanol, rinsed with 1M nitric acid for one minute, triply rinsed with distilled water, and then with ethanol. The pyrite was dried with air and stored briefly in beakers.	(McKibben and Barnes, 1986)
40 – 80 μm	Powders were prepared by grinding in an agate mortar. The oxidation products were eliminated by rinsing with 10^{-2} MHNO3.	(Bonnissel-Gissinger et al., 1998)
74–177 μm	Samples were crushed using an agate mortar and pestle. The crushed pyrite was soaked overnight in hot hydrofluoric acid, washed in deoxygenated deionized water, dried in air, and sieved.	(Kamei and Ohmoto, 2000)
105 – 150 μm	Samples were dry ground in two steps: 1) a glass-cleaned ring pulverizer was used to reduce grain size and 2) an agate mortar was used to crush the particles to the desired particle size range. The ground pyrite was dry sieved. Samples were kept in a glass desiccator under vacuum after preparation to avoid surface oxidation.	(Cruz et al., 2001)
150–250 μm	Pyrite was ground using an agate mortar, sieved with ethanol, and then washed in an ultrasonic bath. Procedure was repeated until the ethanol was clear and free of fine particles after the ultrasonic bath treatment.	(Descostes et al., 2004)
150 – 500 μm	Crushed minerals were sieved, ultrasonically treated and washed repeatedly to remove fine particles, and then treated with 10% HCl for 2 hours to remove any preexisting oxide layer. The crushed mineral particles were rinsed with ethanol and allowed to dry.	(McGuire et al., 2001)
-0.30 mm	Material was classified into various size fractions by wet–dry screening. Prior to leaching experiments, samples of the ground material were soaked in 3 M hydrochloric acid solution for 36 h, filtered, rinsed with double-distilled water, dried with acetone, and kept under vacuum in a desiccator.	(Caldeira et al., 2003)
250 – 420 μm	The pyrite was crushed, sieved, and rinsed with ethyl alcohol three to five times until the supernatant was clear. The samples were then sonicated in ethyl alcohol (repeated at least three times until the supernatant was clear). The grains were dried at 70°C for 12 h.	(Jerz and Rimstidt, 2004)
37 – 74 μm	Pyrite was ground in air for different periods. After grinding, samples were sieved under dry conditions and the size fraction between 200 and 400 mesh collected.	(Sasaki, 1994)

2.2 METHODS

2.2.1 *Crushing and Sieving Procedures*

Sample Crushing: Five pyrite samples, two hydrothermal and three sedimentary in origin, were used to compare the effectiveness of dry and wet sieving techniques. The starting samples were either massive euhedral or nodular (**Table 2**). Nodular samples were cut using a trim saw. For square and rectangular samples, the outside edges were removed to obtain a pristine internal sample. Spherical samples were cut into smaller square/rectangular pieces and the outside surface was removed using 220-mesh silicon carbide grit. Samples of 30-50 g were collected and crushed into pea–size pieces using a sledgehammer. The sledgehammer, steel plate and sample were wrapped in aluminum foil to prevent contamination.

Table 2. Samples used in this study. Composition was determined using x-ray diffraction and molar S:Fe ratio for each sample.

Sample ID	Source	Morphology	Petrogenetic Environment	Mineralogy	Molar S/Fe
HY-001	Wards Natural Science	Euhedral cube	hydrothermal	pyrite	2.01
HY-002	Rock Currier, personal communication	Euhedral cube	hydrothermal	pyrite	2.02
SED-001	Lower Kittanning coal, OH	nodular	sedimentary, within coal	pyrite	2.02
SED-002	Texas	nodular	sedimentary, within coal	pyrite	1.97
SED-003	Calvert Bluff Formation, Texas	spherical nodule	sedimentary, within coal	pyrite with minor quartz	1.97

Powder Preparation and Characterization: Powder preparation techniques using both a mixer mill and a mortar and pestle were evaluated. Most samples of the crushed pyrite (~10 g) were milled into a powder using a tungsten carbide mixer mill for approximately 3 minutes. An aliquot of one sample (HY-001) was also ground in an agate mortar and pestle as a comparison to the mixer mill. Samples were placed in a desiccator under vacuum immediately after being powdered. X-ray diffraction analysis (Philips XRD PW3710; Almelo, Netherlands) indicates that all samples are pyrite, although SED-003 contains minor (≤10%) quartz. Additional aliquots (~0.1 g) of pyrite powder were completely dissolved in 10 mL concentrated nitric acid and further diluted to 5% nitric acid for iron and sulfur analysis by ICP-AES. The results (**Table 2**) indicate that the samples consist of stoichiometric FeS_2, indicating insignificant contribution from other species.

Dry Sieving: Prior to sieving, the sample was dried in an oven for approximately 30 minutes at 105°C to drive off adsorbed moisture. Given the results of previous pyrite oxidation experiments, the appearance of oxidation products on pyrite surfaces is most likely minor, given the short period of time in which the samples were in the oven (Borek Sandra, 1993; Jerz and Rimstidt, 2004). In addition, the samples were treated prior to dissolution experiments to ensure the removal of any possible oxidation products (see section on dissolution experiment procedures). Approximately 5-6 grams of material were transferred to a polypropylene sieve set equipped with nylon mesh (41 μm, 63 μm and 75 μm mesh sizes were used) and shaken for 10 minutes in a sieve shaker. Following the dry sieving procedure, a coating of pyrite grains much finer than the smallest sieve size remained on mineral surfaces. To address this issue, two surface cleaning procedures were evaluated: (1) About 10 grams of sieved pyrite were added to ~200 ml tetrabromoethane (density = 2.89 g/cm^3) within a 250 ml separatory funnel. After 20 minutes, the

settled pyrite was collected from the bottom of the column and cleaned with acetone. (2) Two to three grams of sieved pyrite grains were placed into a 50 ml polypropylene test tube. Approximately 35 ml of 70% ethanol were added to each tube and the sample was ultrasonicated for 1 minute. Suspended material within the solution was decanted and discarded. Following both procedures, the remaining samples were oven-dried 30-60 minutes at 105°C, then transferred to a desiccator and placed under vacuum. Sub-samples were collected for SEM analysis to determine the size range of the particles collected.

Wet Sieving: A vacuum filtration technique was used to obtain multiple fractions of pyrite. In initial experiments, we captured the 63-75 μm size fraction; however, we found that this size range did not provide enough material for our dissolution experiments. The size range was then broadened to capture pyrite particles 44-75 μm in diameter. Three-inch brass sieves, mesh sizes 200 (74 μm), 230 (63 μm) and 325 (45 μm) were inserted tightly within a one-piece porcelain Büchner funnel with a fixed perforated filter (**Fig. 2**). Whatman No. 54 filter paper at the base of the Büchner funnel was used to trap material finer than 20 microns. A rubber crucible adapter was used to ensure a tight seal between the funnel and 500 ml Pyrex side arm flask. Tygon tubing (3/8 x 1/8 inch) was used to connect this set-up to a water trap. The water trap consisted of another 500 ml side arm flask connected to Tygon tubing using a 6.5 rubber stopper with a removable glass stem. Each of the Pyrex side arm flasks were attached to support stands using adjustable angle clamps. The water trap was connected to a vacuum pump, which was necessary for sufficiently rapid sieving.

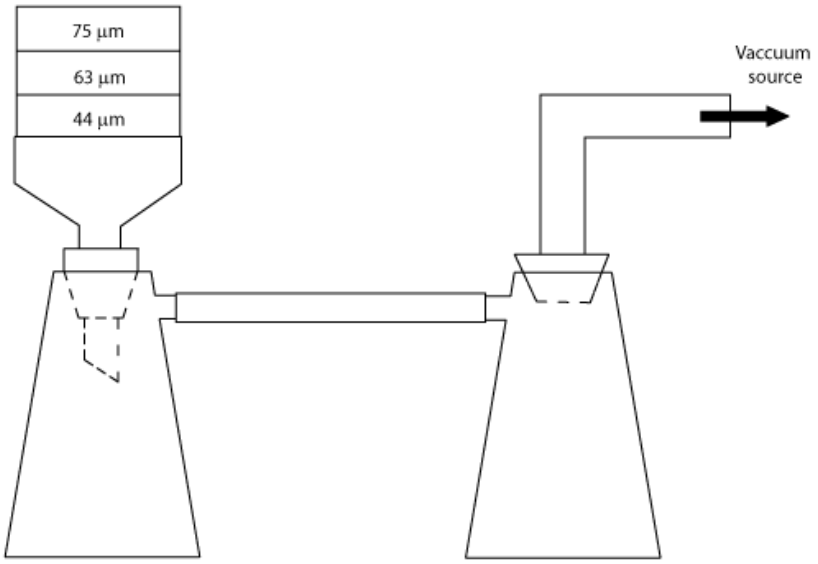

Figure 2. Wet sieving apparatus. Size fractions are collected using an adapted vacuum filtration technique.

To begin the procedure, powdered material was transferred into 50-ml polypropylene test tubes. Ethanol (35 ml of 70%) was then added to each tube and the sample was ultrasonicated for 1 minute. The material was then poured onto the top of the sieve stack to begin the wet sieving process. Alternating aliquots of ultrapure water and 50% ethanol (ending with ethanol) were added until the entire sample had been sieved. Ethanol was used to prevent pyrite oxidation during sieving. Finally, the remaining samples were oven-dried 30-60 minutes at 105°C, then transferred to a desiccator and placed under vacuum. Sub-samples were collected for SEM analysis to determine the size range of the particles collected.

Samples SED-001 and SED-002, both of which were extracted from a coal matrix, appeared to contain a significant fraction of organic carbon (not revealed during XRD analyses), based on the formation of an opaque black solution after addition of 5 mL concentrated nitric acid to approximately 1 gram of a powdered pyrite sample. This phenomenon was also observed by Lord (Lord, 1982). Based on the method of Huerta-Diaz and Morse (Huerta-Diaz and Morse,

1990), these samples were treated with concentrated H_2SO_4 for approximately 10 minutes and rinsed with ultrapure water, followed by ethanol. This appeared to eliminate the organic carbon.

2.2.2 *Dissolution Experiments*

The dissolution behavior of pyrite material that had undergone dry sieving was compared to the dissolution of those that had been wet sieved. Prior to experimentation, all pyrite samples were treated to remove any surface iron oxides or iron sulfates that could have been produced when the samples were exposed to the atmosphere. This procedure, a modified version of a method used by Paschka and Dzombak (Paschka, 2004), involved boiling 7-8 g of pyrite in 50 ml concentrated HCl for approximately 10 minutes. The sample was rinsed with boiling concentrated HCl at least twice, then rinsed with 25 ml deionized water, followed by a boiling acetone rinse using a vacuum filter. The acetone rinse was repeated at least 3 times. The sample was dried in the oven at 105°C for about 10 minutes and stored in a desiccator. Specific surface area measurements were conducted prior to the cleaning procedure.

Dissolution experiments were carried out in a batch reactor under tightly controlled conditions: pH = 3±0.05, a constant temperature of 25±0.01°C, fixed dissolved oxygen (8-11ppm), and electrolyte solution of 0.01 M NaCl initial ionic strength. A precise 5.355±0.005g aliquot of cleaned pyrite was added to 1.5 L of deionized water in a stirred, jacketed glass vessel with a lid having sealed ports for insertion of reagents and withdrawal of samples from the reactor. During the experiments, the reactor was covered with aluminum foil to exclude light. pH was maintained through the addition of HCl or NaOH via acid/base pumps and a pH-stat. Pyrite dissolution was monitored by measuring total dissolved iron. Five milliliters of sample were collected periodically over an 8 hour time period, and then filtered through a 0.45 μm disposable

filter into a 20 ml polyethylene scintillation vial containing 5 ml 10% HNO_3 for sulfur and iron analysis. Iron and sulfur concentrations were measured using ICP-AES, with replicate measurements of Fe by flame and graphite furnace AA.

2.2.3 *Analytical Methods*

Specific surface area of each sample was measured by the nitrogen adsorption multipoint BET method with a Quantosorb instrument (Quanta Chrome, Boynton Beach, Florida). The accuracy of the instrument was verified by measurements on alumina and black carbon standards of known surface area. Particle surfaces were examined pre- and post- cleaning using a Philips XL-30 FEG field emission scanning electron microscope (Almelo, Netherlands). Sulfur and iron concentrations were measured on a SpectroFlame EOP ICP-AES (Kleve, Germany) using EPA Method SW 846. Accuracy of measurements are within $\pm$5% of true values. Replicate analyses of total dissolved iron were measured using a GBC 908AA atomic absorption spectrometer (GBC Scientific Equipment, Hampshire, IL). Instrument calibration was carried out using a suite of different concentrations of iron standard solution (Fisher Scientific) in 5% nitric acid matrix. All the aqueous samples were preserved in 5% nitric acid matrix before ICP-AES and AA measurements.

2.3 RESULTS

SEM analyses of dry sieved samples indicated the presence of significant numbers of particles smaller than the desired range, *i.e.*, <44 μm (**Fig. 3a, c**). In contrast, the wet sieving

preparation method was successful at concentrating the intended particle size range and cleaning the surfaces (**Fig. 3b, d**). The addition of the tetrabromoethane cleaning step to the dry sieved samples reduced the number of <44 μm particles, but still left substantial numbers of fine particles (**Fig. 4a**). The ultrasonicating cleaning procedure was also largely unsuccessful in removing finer pyrite particles in the dry sieving method, based on SEM observation (**Fig. 4b**).

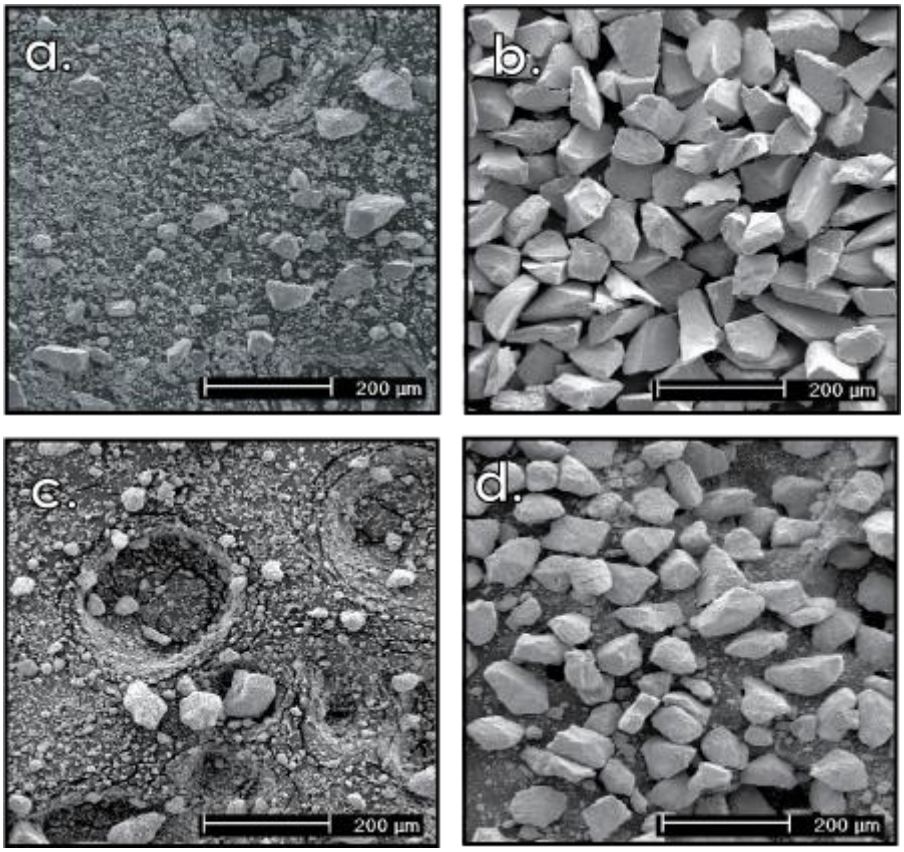

Figure 3. Comparison of results obtained using the wet sieving technique and the dry sieving technique. The wet sieving technique was successful in eliminating the aggregation of smaller size particles, achieving a narrow range of particle sizes for all samples, and removing adhering particles from the pyrite surface. a) Dry sieved, 63-75 μm, hydrothermal pyrite sample, HY-001, 63-75 μm, and b) HY-001, wet sieved, target size fraction 63-75 μm. c) Dry sieved, 44-75 μm, sedimentary pyrite sample, SED-002, and d) SED-002, wet sieved, target size fraction 44-75 μm .

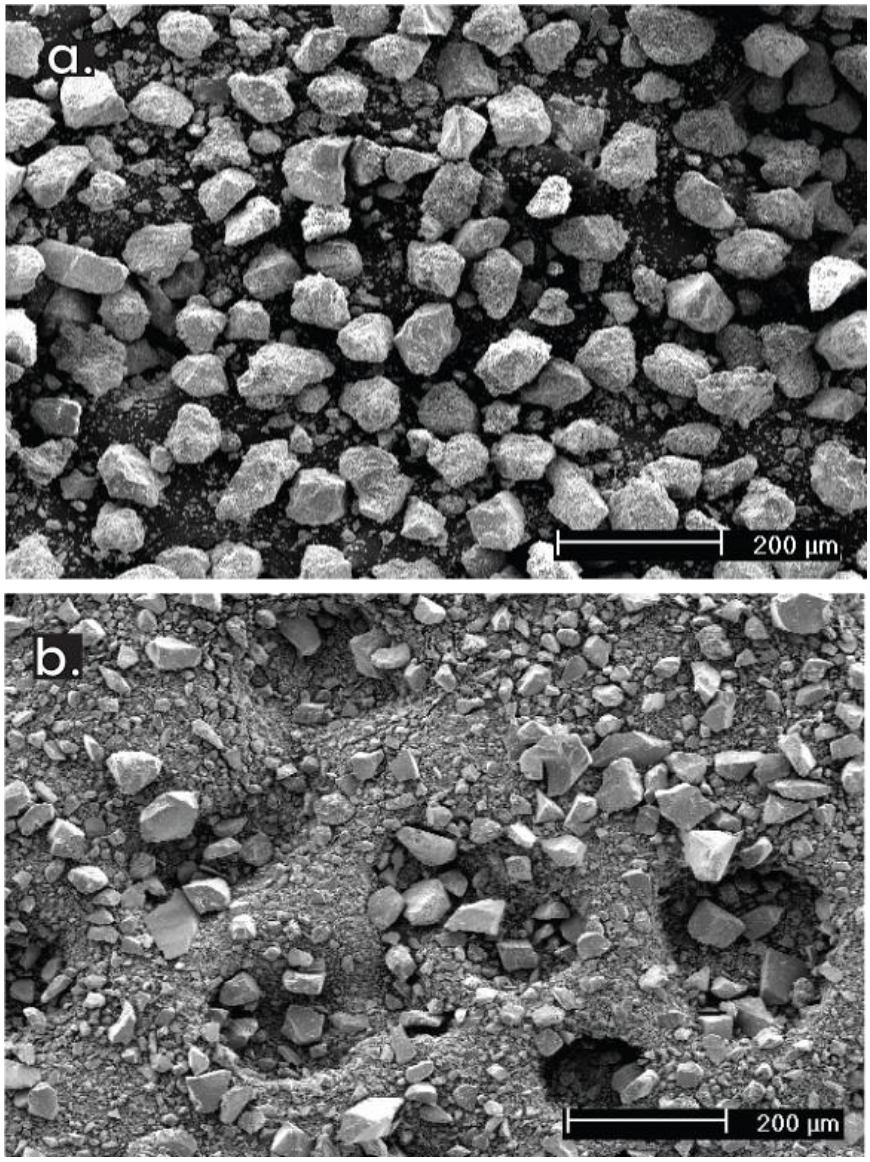

Figure 4. Dry sieved samples after cleaning steps. Sedimentary pyrite sample SED-003 showed some improvement after the tetrabromoethane cleaning procedure, although particles smaller than the finest sieve size (44 µm) clearly still remain. b**) Hydrothermal pyrite HY-002 showed little improvement after ultrasonication cleaning procedure. See text for details of procedures**

BET surface area measurements on dry sieved samples (63-75 μm) yielded a range from 0.2 to 3.1 m^2/g, with SED-003>HY-001>SED-001>SED-002 (**Table 3**). Surface area measurements for wet sieved samples (44-75 μm) ranged from 0.2 to 5.4 m^2/g, with SED-002>SED-001>SED-003>HY-001. The BET surface area of the dry sieved samples was surprisingly low, given the large number of fine particles observed by SEM. We note, however, that the BET method has a relatively high uncertainty at low surface area values. Further work needs to be undertaken to more fully address why the wet sieved material shows a larger apparent range of measured BET surface area values.

Results of the dissolution experiments are reported in **Table 3**. Initial dissolution rates (**Table 3**) were calculated using iron concentrations measured one hour into the experiment. Dissolution rates calculated for dry sieved pyrite samples were highest for sedimentary samples and lowest for hydrothermal samples, with SED-002>SED-003>SED-001>HY-001. Dissolution rates obtained for hydrothermal samples yielded the lowest rates, regardless of whether they were wet or dry sieved. The highest dissolution rates were obtained from sedimentary samples that had been prepared using the dry sieve technique.

Table 3. Surface area and dissolution rates for pyrite samples after preparing material using the dry and wet sieving technique. Based on measurements of black carbon and alumina standard materials, the estimated maximum error for surface area measurements is $\pm$0.6 m^2/g.

	Dry Sieving Preparation 63 – 75 μm		Wet Sieving Preparation 45 – 75 μm	
Sample ID	**Initial Dissolution Rate** *μg of Fe/min*	**Surface Area** m^2/g	**Initial Dissolution Rate** *μg of Fe/min*	**Surface Area** m^2/g
HY-001	34.1	1.9	3.8	0.22
HY-002	*na*	*na*	*na*	*na*
SED-001	70.4	0.90	21.1	2.8
SED-002	82.3	0.20	23.4	5.4
SED-003	81.8	3.1	0.02	0.42

For wet sieved pyrites, the ranking of relative dissolution rates was similar to that of the dry sieved sedimentary pyrites, with SED-001>SED-002>SED-003>HY-001>HY-002. However, samples that were dry sieved achieved far higher absolute dissolution rates than those that were wet sieved (**Fig. 5**), even though the dry sieved samples were nominally sieved to a narrower particle size range (63-75 μm *vs*. 44-75 μm for wet sieved samples). A comparison of grinding techniques for sample HY-001 indicate that the rate of pyrite dissolution is higher for the sample powdered with the mixer mill than for the one prepared with the mortar and pestle (**Fig. 6**). SEM results suggest that machine grinding yielded a greater portion of grains skewed toward the lower end of the sieved size range, thus resulting in more exposed surface area and a higher dissolution rate.

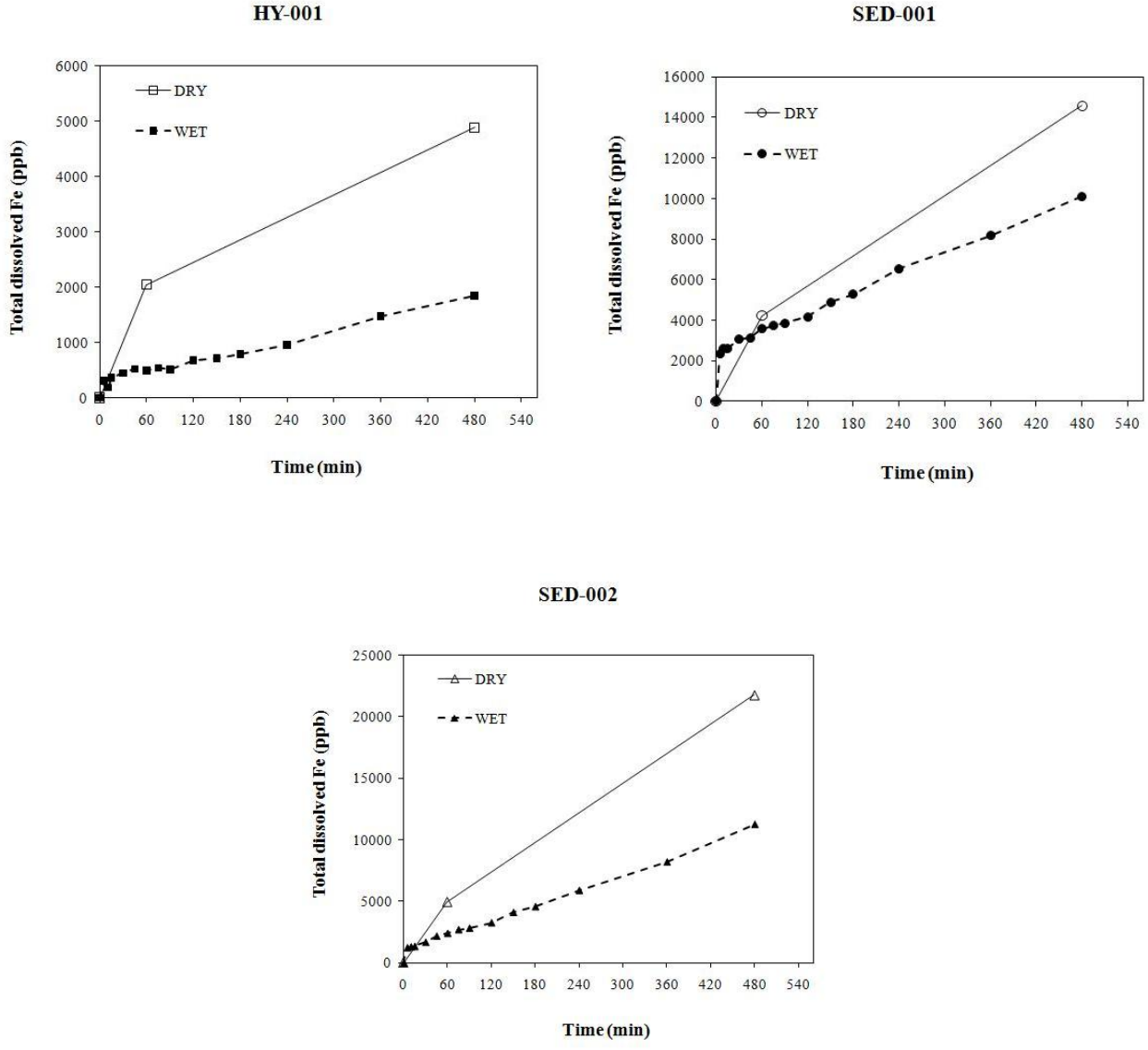

Figure 5. Dissolution results for pyrite samples. Dissolution results for three pyrite samples (one hydrothermal and two sedimentary) following preparation by dry and wet sieving. Samples were initially ground using a mixer mill. Dry sieved samples show much higher dissolution rates than samples that were wet sieved

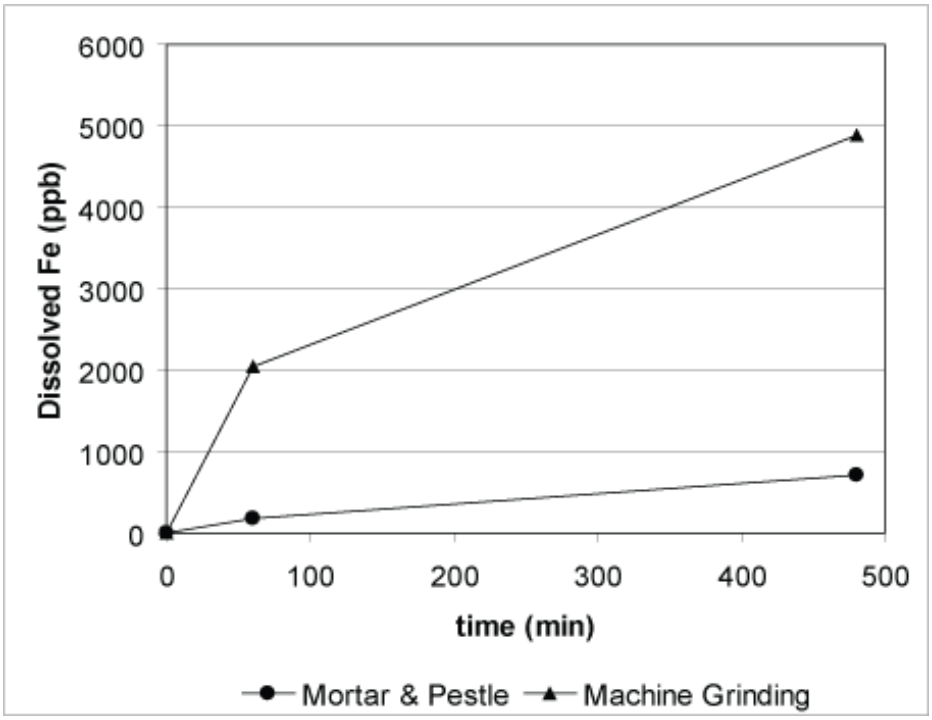

Figure 6. Comparison of cumulative iron concentration as a function of time for 63-75 μm splits of pyrite HY-001 produced by different grinding methods: hand grinding using an agate mortar and pestle vs. machine grinding using a mixer mill. In both cases, the ground samples were wet sieved.

2.3.1 *Dry sieving vs. wet sieving of crushed pyrite*

Early efforts using the dry sieving technique to achieve a narrow range of fine particles yielded poor results; dry sieving resulted in a wide range of sizes from very fine particles adhering to the surface of individual grains to smaller particles (<44 μm) scattered throughout the larger matrix. Initially we attributed the aggregation of smaller sized particles to electrostatic charges being induced across the nylon mesh material, thus prohibiting movement through the sieve mesh, while the samples were sieved using the sieve shaker. However, changing from the polypropylene sieves to brass sieves did not improve the yield. The addition of tetrabromoethane

to the sieving procedure helped marginally when the tetrabromoethane followed dry sieving, as the tetrabromoethane tended to clear the particle surfaces of finer particles. However, the finer particles were not removed from the sample, and using tetrabromoethane prior to dry sieving had little to no effect on the distribution of particles in the final sample.

Several workers ultrasonicated their respective samples in aqueous suspensions after dry sieving to remove fine particles from the pyrite surface (Hammack RW, 1988; McGuire et al., 2001; McKibben and Barnes, 1986). However, this is not an effective particle separation method for fine grained (<100 μm) samples. Particles within our range of interest (45-75 μm) tend to remain suspended in the solution after ultrasonication. Decantation removes these particles along with other fine particles, ultimately biasing the method to retain larger sized particles within the collected size range.

The wet sieving technique was significantly more successful in producing a uniform distribution of particles in the size range of interest and is an effective method to produce a uniform, fine, and restricted pyrite particle size range for experiments. In addition, this technique does not require a post–processing cleanup step to remove adhering particles, as the particles are removed during the wet sieving procedure.

2.3.2 *Application to pyrite dissolution experiments*

Results from the dissolution experiments indicate that pyrite preparation methods can affect the rate of dissolution significantly (**Fig. 5**). Pyrite powder prepared by dry sieving exhibited the highest surface area measurements and dissolution rates of all samples. Examination by SEM indicates that these results are likely caused by the presence of particles

finer than 63 μm that adhere to larger particles even after separation with tetrabromoethane, and regardless of the type of sieve used.

2.4 CONCLUSIONS

There is clearly a need to standardize sample preparation techniques to allow accurate comparisons of pyrite dissolution experiments under diverse conditions. We have developed a wet sieving procedure using vacuum filtration techniques to obtain fine (<100 μm) particle size fractions of pyrite for use in geochemical experiments. Compared to traditional methodologies, this procedure is far more successful at acquiring a narrow range (45-75μm) of pyrite particles, as reflected in batch dissolution experiments and SEM analysis. This method uses readily available materials and equipment, and has potential application to other minerals as well.

This manuscript was accepted for publication:* ***Wolfe, A.L**., Liu, R., Stewart, B.W., Capo, R.C., and Dzombak, D.A. (2007) A method for generating uniform size-segregated pyrite particle fractions. Geochemical Transactions* ***8****:9.*

ACKNOWLEDGEMENTS:

We gratefully acknowledge the staff and faculty associated with the Materials Micro-Characterization Laboratory of the Department of Materials Science and Engineering, University of Pittsburgh, for assistance with the x-ray diffraction and scanning electron microscopy conducted during this study. We thank W. Winters, Office of Surface Mining, and R. Currier for providing pyrite samples, and B.K. Games for technical support with the ICP-AES analyses. This manuscript benefited greatly from the detailed comments and suggestions of three anonymous reviewers. This work was supported by NSF EAR-0229019, 0214212, and 0517313 (R. C. Capo/B. W. Stewart), NSF EAR-0228903 (D. A.

Dzombak), NASA Astrobiology Institute/Penn State Astrobiology Research Center (B. W. Stewart/R. C. Capo), and the Ji-Dian Liang Fellowship (R. Liu).

3.0 IRON ISOTOPE INVESTIGATION OF HYDROTHERMAL AND SEDIMENTARY PYRITE AND THEIR AQUEOUS DISSOLUTION PRODUCTS

3.1 INTRODUCTION

Iron sulfides constitute a diverse group of solid and dissolved complexes within aquatic systems. Pyrite (FeS_2), the most common sulfide mineral in Earth's surface environments, is found in a wide variety of geologic environments. It can form under high temperature conditions, including contact metamorphism and hydrothermal fluid circulation, and in low temperature (<100°C) sedimentary environments. Within sedimentary environments, pyrite is known as a redox buffer in anoxic conditions and its presence is a strong indicator of reducing conditions (Descostes et al., 2004). These sulfides are essential in regulating and controlling the global geochemical iron and sulfur cycles. They demonstrate significant complexity within low temperature environments in which a number of metastable phases become significant in biogeochemical processes (Rickard and Luther, 2007). In addition, sulfides are the major contributor to acid mine drainage (AMD), which is a serious problem in coal and metal mining regions.

In order to effectively interpret sulfide geochemistry in the geologic record and to understand the interaction of pyrite with aqueous environmental fluids, the processes and mechanisms governing pyrite dissolution need to be understood. Most experimental studies of pyrite dissolution have been conducted with hydrothermal pyrite. These have shown that the rate of

pyrite oxidation is dependent on factors such as pH, dissolved oxygen, ferric iron concentrations and the presence of iron- or sulfur-oxidizing bacteria. Rates of oxidation estimated in field systems can differ substantially, but often rates are much higher because dissolution of sedimentary pyrite present in coal systems is accelerated in the presence of bacteria.

There is a strong need to develop new methods to study pyrite dissolution in order to increase our knowledge of dissolution mechanisms, enable more accurate reaction rate measurements, and to improve our ability to predict the temporal evolution of ground and surface water that has come into contact with pyrite. Innovative developments in mass spectrometry now provide researchers opportunities to explore transition metal isotope systems, such as iron (Anbar et al., 2000; Beard and Johnson, 1999; Brantley et al., 2001; Bullen et al., 2001; Johnson and Beard, 1999). In this study, the ability to quantify and source-track the dissolution of pyrite within AMD systems is evaluated using iron isotopes.

The sequential history of iron mobilization and mass transfer are among causal factors that can contribute to iron-isotope fractionation in low-temperature geological settings. Isotopes of iron are fractionated during biogenic and inorganic redox processes, complexation with soil organic matter, bacterial interactions, and during surface adsorption and mineral precipitation reactions (Borrok et al., 2009) and references therein). Iron isotopes have been used as a tool to examine source and mechanisms of controlling Fe cycling in freshwater environments and soils (Bergquist and Boyle, 2006; Borrok et al., 2009; Emmanuel et al., 2005; Fantle and DePaolo, 2004; Ingri et al., 2006), and more recently, during oxidative weathering of sulfide rich rocks and minerals (Borrok et al., 2009; Fernandez and Borrok, 2009; Herbert and Schippers, 2008). Theoretical estimates using Mössbauer and vibrational spectroscopy predict significant fractionation effects occurring between pyrite and ferrous iron (Polyakov and Mineev, 1999); however, interpretations remain somewhat unclear given the lack of experimental determination

of Fe fractionation factors associated with pyrite formation and dissolution (Severmann et al., 2006).

In this study, we investigate the range of iron isotope values in pyrite from Phanerozoic coal and sedimentary fossil replacement structures to evaluate the utility of this system as a tracer of Fe in acid mine drainage situations. In addition, iron isotopes were used to study dissolution rates of different pyrite types (hydrothermal, fossil replacement, and coal nodules). This is the first investigation of iron isotope fractionation occurring during pyrite oxidation in a well-constrained experimental setting.

3.2 METHODS

3.2.1 *Samples and Characterization*

Eight pyrite samples, three hydrothermal and five sedimentary, were obtained from various sources; morphology and geological origins are provided in **Table 7**. The starting samples were either massive euhedral or nodular. Sedimentary pyrite samples included fossil replacements (ILPS-1, INND-1) and nodular pyrite collected from coal seams (PAND-1, TXND-3, TXND-4). Pyrite samples were crushed, milled, and wet sieved using a procedure developed by Wolfe et al. (2007) to obtain 45-75 μm fractions for use in dissolution experiments.

Specific surface area of each sample was measured by the nitrogen adsorption multipoint BET method with a Quantosorb instrument (Quanta Chrome, Boynton Beach, Florida). The accuracy of the instrument was verified by measurements on alumina and black carbon standards of known surface area. Particle surfaces were examined pre- and post- cleaning using a Philips XL-30 FEG field emission scanning electron microscope (Almelo, Netherlands).

Table 4. Characteristics of pyrite samples used in this study. Composition was determined using x-ray diffraction and molar S:Fe ratio of each sample.

Sample ID	Source/ Location	Morphology	Petrogenetic Environment	Mineralogy	Specific Surface Area (m^2/g)
HY-Paschka	Hubbard Scientific	Nodular	Hydrothermal	Pyrite	0.22
HY-PERU4	Peru	Nodular	Hydrothermal	Pyrite	0.10
HY-SPN2A	Spain	Nodular	Hydrothermal	Pyrite	0.07
ILPS-1	Illinois, USA	Nodular *(pyrite sun)*	Sedimentary; Between shale and coal seams; fossil replacement	Pyrite	0.35
INND-1	New Albany Shale; Illinois, USA	Nodular	Sedimentary; fossil replacement	Pyrite	0.21
PAND-1	Pennsylvania, USA	Nodular	Sedimentary, within coal	Pyrite	2.82
TXND-3	Texas, USA	Nodular	Sedimentary, within coal	Pyrite with minor quartz	0.42
TXND-4	Texas, USA	Nodular	Sedimentary, within coal	Pyrite	5.37

3.2.2 *Bulk Pyrite Sample Dissolution*

Aliquots of the 45-75 µm starting materials were dissolved in warm nitric acid, and splits were taken for trace element and iron isotope analyses, as described below. The remainder of the 45-75 µm material was used for oxidative dissolution experiments, as reported by Liu et al., (2008).

3.2.3 *Dissolution Experiment Setup*

For each pyrite sample, continuous batch experiments were conducted and the rate of dissolution was studied in a batch reactor under tightly controlled conditions: pH = 3±0.05, a constant temperature of 25±0.01°C, fixed dissolved oxygen (8–11 ppm), and electrolyte solution of 0.01 M NaCl initial ionic strength (Liu et al., 2008). Prior to experimentation, all pyrite samples were treated to remove any surface iron oxides or iron sulfates that could have been produced when the samples were exposed to the atmosphere. This procedure, a modified version of a method used by Paschka and Dzombak (2004), involved boiling 7–8 g of pyrite in 50 ml concentrated HCl for approximately 10 minutes. The sample was rinsed with boiling concentrated HCl at least twice, then rinsed with 25 ml deionized water, followed by a boiling acetone rinse using a vacuum filter. The acetone rinse was repeated at least 3 times. The sample was dried in the oven at 105°C for about 10 minutes and stored in a desiccator. Specific surface area measurements were conducted prior to the cleaning procedure. Aliquots of the bulk sample were collected for iron isotope analysis prior to dissolution experiments.

A precise 5.355±0.005 g aliquot of cleaned pyrite was added to 1.5 L of deionized water in a stirred, jacketed glass vessel with a lid having sealed ports for insertion of reagents and withdrawal of samples from the reactor. During the experiments, the reactor was covered with aluminum foil to exclude light. A constant pH was maintained through the addition of HCl or NaOH via acid/base pumps and a pH-stat. The concentration of dissolved oxygen was maintained at 9-12 ppm ($10^{-3.55}$ – $10^{-3.43}$ mol/L) by controlling the oxygen partial pressure in the reactor headspace.

Pyrite dissolution was monitored by measuring total dissolved iron in the leachate. Five milliliters of sample were collected periodically over a 24 hour time period, and then filtered

through a 0.45 μm disposable filter into a 20 ml polyethylene scintillation vial containing 5 ml 10% HNO_3 for sulfur and iron elemental analysis. A three-way stopcock was used for sampling to ensure the headspace of the reactor would remain unaffected by the outside environment during the experiments.

3.2.4 *Elemental Analyses*

Sulfur and iron concentrations in both the bulk pyrite and the experiment leachates were measured on a SpectroFlame EOP ICP-AES (Kleve, Germany) using EPA Method SW 846 (EPA). Accuracy of measurements are within ±5% of true values. Replicate analyses of total dissolved iron in the experiment leachates were measured using a GBC 908AA atomic absorption spectrometer (GBC Scientific Equipment, Hampshire, IL). Instrument calibration was carried out using a suite of different concentrations of iron standard solution (Fisher Scientific) in 5% nitric acid matrix. All the aqueous samples were preserved in 5% nitric acid matrix before ICP-AES and AA measurements. In the bulk sample solutions, abundances of more than 40 trace elements were analyzed by ICP-MS **(**Activation Laboratories Ltd., Ontario, Canada).

3.2.5 *Isotopic Analyses*

Aliquots of leachate samples from each pyrite dissolution experiment were collected for iron isotope analysis at 1, 8 and 24 hours from the start of the experiment, with the exception of sample HY-SPN2A, in which the first sample was collected at 6 hours. Iron separations were conducted in a laminar flow clean hood based on a procedure modified after Bullen et al.

(2001b). Aliquots containing at least 20 μg of Fe were evaporated to dryness in Teflon containers and redissolved in 5 mL of 6.0 N HCl for anion exchange chromatography. The solution was loaded onto an anion exchange column (BioRad AG1X8) previously cleaned with alternating 1.0 N HCl and ultrapure water. The resin was then conditioned using 6 ml of 6.0 N HCl. After the sample solution had been loaded on the resin, the matrix was removed in 11 ml of 6.0 N HCl and 1 ml of ultrapure water. The Fe was eluted with alternating 1 ml aliquots of 1.0 N HCl and ultrapure water, evaporated to dryness, and then the column separation procedure was repeated. After going through the column a second time, the sample was evaporated to dryness and redissolved in 2% HNO_3 for MC-ICP-MS analysis.

Chemistry blanks and yields of the dissolution and chemical separation on anion-exchange columns of various samples were measured by ICP-AES at the University of Pittsburgh. The overall chemistry blanks were <100 ng.

Isotopic ratios were measured at Arizona State University using a Thermo Neptune MC-ICP-MS. Solutions were analyzed by MC-ICP-MS at a concentration of 2-3 ppm Fe with a Cu spike added to correct for instrumental mass bias (Arnold et al., 2004; Marechal et al., 1999). Sample solution duplicates and one procedural blank were analyzed for each petrogenetic group of samples. All Fe isotopes values reported reflect the average of the replicate measurements. The ratios $^{56}Fe/^{54}Fe$ and $^{57}Fe/^{54}Fe$ were measured simultaneously; analyses that did not demonstrate the expected mass-dependent relationship between these ratios were rejected. Isotopic ratios are expressed in standard delta notation (in units of per mil, ‰) relative to the international IRMM-014 Fe standard:

$$\delta^{56}Fe = [(^{56}Fe/^{54}Fe_{sample}/^{56}Fe/^{54}Fe_{IRMM}) - 1] \times 1000 \quad (1)$$

The external precision of the measurements was better than 0.1‰.

3.3 RESULTS

3.3.1 *Bulk pyrite sample characterization*

X-ray diffraction analysis (Philips XRD PW3710; Almelo, Netherlands) indicates that all samples are pyrite, although TXND-4 contains minor (≤ 10%) quartz. Chemical analyses of Fe and S concentrations in bulk sample dissolution indicate that the samples consist of stoichiometric FeS_2. Chemical analysis of more than 40 trace elements showed that hydrothermal pyrite samples generally contained more Co, Bi and Te, and less Tl, Ba, Rb and Sr than the sedimentary pyrite samples (**Table 5**). The three sedimentary samples associated with coal contained more Hg compared to the other sedimentary pyrite and hydrothermal pyrite samples.

3.3.2 *Leaching Experiments: Aqueous Chemistry vs. Time*

The abiotic, oxidative dissolution of pyrite of different petrogenetic origins (*e.g.*, nodules in coal beds, massive hydrothermal crystals) was studied in a batch reactor system under oxic conditions maintained by a controlled supply of dissolved oxygen (9-12 mg/L) at fixed pH. Experimental results of pyrite oxidation at pH = 3 show that pyrite from different geologic environments exhibits unique dissolution behavior (Liu et al., 2008). Results show an increase in total dissolved iron over the 24 h experiment period (**Table 6**). All iron measured in these experiments is assumed to be ferrous iron, based on previous experimental work with

hydrothermal pyrite under the same conditions in which no ferric iron was detected at any time during the experiment (Paschka and Dzombak, 2004; Liu et al., 2008). Based on the total dissolved iron released over the experimental period, sedimentary pyrite samples collected from coal dissolved much faster than the other pyrite samples, with TXND-4 > PAND-1 > TXND-3 > HY-PASCHKA > ILPS-1 > INND-1 > HY-SPN2A > HY-PERU4 (see **Table 7** for sample descriptions). The extent of dissolution was similar for the hydrothermal pyrite samples and the other two sedimentary samples (ILPS-1, INND-1). Total dissolved sulfur concentrations were also monitored over the experimental period. Total dissolved sulfur increased over time for all pyrite samples (**Table 6**). Ion chromatography (IC) analysis showed that sulfate was the only oxidized sulfur species present. See Liu et al. (2008) for additional details.

Table 6 also shows the molar ratios of total iron to total sulfur in the experimental solutions at 1, 8, and 24 hours. A molar S:Fe ratio of 2:1 is expected from pyrite stoichiometry, and results demonstrate pyrite is not dissolved stoichiometrically, at least in the early stages of dissolution. The S/Fe ratio of all samples increases over the duration of the experiment (**Fig. 7**), with the exception of sample TXND-4, which stays approximately constant at a S/Fe ratio of ~1.7. The overall results are consistent with the pyrite oxidation experiments of Descostes et al. (2004), and indicate that either excess Fe (not bound to S) is present on the pyrite surface, or that sulfur is held on the mineral surface after pyrite dissolution (Liu et al., 2008).

Table 5. Trace element concentrations in bulk pyrite samples. Where indicated, minimum (<) and maximum (>) values fell outside the limits of quantification by ICP-MS. DL = detection limit.

Element	DL	HY-PASCH	HY-PERU4	HY-SPN2A	ILPS-1	INND-1	PAND-1	TXND-3	TXND-4
	µg/L	µg/g	µg/g	µg/g	µg/g	µg/g	µg/g	µg/g	µg/g
Ag	0.200	0.638	0.703	0.188	1.96	< 0.177	< 0.054	0.080	< 0.049
As	0.030	> 25	20.1	4.43	> 64	32.2	> 54	> 53	> 49
Al	2.00	23.0	31.2	> 313	259	401	305	531	276
Au	0.002	0.003	0.001	0.007	0.001	0.004	< 0.001	0.001	< 0.000
Ba	0.100	0.025	0.068	0.454	4.20	20.5	8.35	23.9	4.00
Be	0.100	0.110	< 0.014	0.031	< 0.032	< 0.089	0.081	0.133	< 0.025
Bi	0.300	17.7	10.6	19.4	< 0.096	< 0.266	< 0.081	< 0.080	< 0.074
Br	3.00	3.31	3.51	3.60	8.02	23.9	7.84	6.10	6.17
Ca	700	602	149	1,816	289	2,569	189	398	197
Cd	0.010	0.028	0.115	0.072	0.385	0.080	0.351	0.082	0.257
Co	0.005	> 25	14.3	> 31	7.92	13.4	0.250	12.6	0.708
Cr	0.500	0.872	0.270	5.89	5.81	2.30	1.41	10.8	0.740
Cs	0.001	0.041	0.002	0.044	0.076	0.202	0.311	0.441	0.107
Cu	0.200	> 25	> 27	> 31	> 64	> 177	> 54	> 53	> 49
Ga	0.010	0.129	0.120	0.774	0.542	0.673	0.159	1.79	0.141
Ge	0.010	0.163	0.406	0.465	0.693	1.27	0.235	0.602	0.286
Hf	0.001	0.003	0.001	0.074	0.042	0.019	0.029	0.176	0.021
Hg	0.200	< 0.025	0.041	0.047	0.257	< 0.177	3.05	3.34	8.63
K	30.0	6.14	20.3	48.5	199	434	132	870	78.9
I	1.00	0.246	0.135	< 0.157	< 0.321	< 0.886	0.270	0.265	0.247
In	0.001	0.128	0.223	0.003	0.001	0.001	0.007	0.019	0.005
Li	1.00	0.246	0.135	5.17	< 0.321	< 0.886	0.270	7.17	< 0.247
Mg	1.00	134	45.8	576	42.7	284	22.4	2545	13.8
Mn	0.100	104	0.257	27.6	3.79	133	1.22	56.8	3.13
Mo	0.100	0.663	0.095	0.141	33.7	13.2	24.9	3.87	14.5

Table 5., *continued*

Element	DL	HY-PASCH	HY-PERU4	HY-SPN2A	ILPS-1	INND-1	PAND-1	TXND-3	TXND-4
	µg/L	µg/g	µg/g	µg/g	µg/g	µg/g	µg/g	µg/g	µg/g
Na	5.00	12.3	5.95	13.0	67.7	201	118	67.1	88.8
Nb	0.005	0.009	0.024	0.118	0.017	0.032	0.027	0.133	0.014
Ni	0.300	69.6	4.22	> 157	75.1	180	1.27	69.8	1.83
Os	0.002	< 0.000	< 0.000	< 0.000	< 0.001	< 0.002	< 0.001	< 0.001	< 0.000
Pb	0.010	4.10	19.1	17.1	> 64	12.5	8.43	20.0	15.5
Pt	0.300	0.037	0.041	< 0.047	< 0.096	< 0.266	< 0.081	< 0.080	< 0.074
Rb	0.005	0.028	0.089	0.246	0.937	1.75	1.02	3.87	0.518
Re	0.001	0.021	0.002	0.000	0.019	0.003	0.001	< 0.000	0.000
Ru	0.010	0.108	0.003	0.052	0.006	0.027	0.003	0.003	0.007
Sb	0.010	0.363	1.14	0.438	12.0	0.248	0.022	1.06	0.407
Sc	1.00	< 0.123	< 0.135	0.626	< 0.321	< 0.886	0.270	1.59	< 0.247
Se	0.200	> 31	12.0	22.5	76.4	13.1	8.38	> 66	7.97
Si	200	< 25	< 27	250.5	257	354	108	451	98.7
Sn	0.100	0.626	> 11	0.532	0.289	0.177	2.38	0.239	1.16
Sr	0.040	0.366	0.406	0.919	0.645	6.09	2.12	5.39	2.12
Ta	0.001	0.001	0.019	0.013	0.004	0.011	0.002	0.005	0.003
Te	0.100	18.9	13.8	1.32	< 0.032	0.089	< 0.027	< 0.027	< 0.025
Th	0.001	0.073	0.006	2.69	0.209	0.098	0.443	3.24	0.104
Ti	0.100	0.675	0.351	39.9	8.66	3.45	15.0	67.9	4.42
Tl	0.001	0.006	0.006	0.011	> 6.4	1.408	> 5.4	> 5.3	> 4.9
U	0.001	0.317	0.319	0.366	0.236	0.044	0.032	0.525	0.020
V	0.100	0.540	> 6.8	2.69	4.75	2.04	0.757	11.4	0.493
W	0.020	> 2.5	> 2.7	> 3.1	> 6.4	> 18	2.37	> 5.3	> 4.9
Y	0.003	0.399	0.036	1.19	0.172	0.315	0.411	2.47	0.226
Zn	0.500	12.1	> 34	26.1	18.8	64.7	15.4	38.0	23.0
Zr	0.010	0.104	0.019	2.43	1.70	0.709	0.797	5.49	0.668

Table 5., *continued*

RARE EARTH ELEMENTS									
Element	**DL**	**HY-PASCH**	**HY-PERU4**	**HY-SPN2A**	**ILPS-1**	**INND-1**	**PAND-1**	**TXND-3**	**TXND-4**
	µg/L	µg/g	µg/g	µg/g	µg/g	µg/g	µg/g	µg/g	µg/g
La	0.001	0.198	0.007	0.302	0.104	0.187	0.711	6.263	0.077
Ce	0.001	0.658	0.026	0.709	0.227	0.407	1.82	13.1	0.243
Pr	0.001	0.111	0.003	0.095	0.026	0.055	0.202	1.50	0.023
Nd	0.001	0.449	0.019	0.437	0.096	0.221	0.792	5.55	0.103
Sm	0.001	0.068	0.009	0.236	0.021	0.057	0.157	1.07	0.028
Eu	0.001	0.028	0.002	0.105	0.004	0.014	0.028	0.255	0.007
Gd	0.001	0.074	0.010	0.344	0.021	0.059	0.135	1.02	0.037
Tb	0.001	0.010	0.002	0.054	0.003	0.009	0.017	0.128	0.006
Dy	0.001	0.054	0.009	0.276	0.023	0.049	0.075	0.581	0.033
Ho	0.001	0.011	0.002	0.048	0.006	0.009	0.012	0.096	0.007
Er	0.001	0.034	0.005	0.132	0.021	0.023	0.035	0.268	0.020
Tm	0.001	0.005	0.001	0.019	0.004	0.004	0.004	0.033	0.003
Yb	0.001	0.036	0.005	0.140	0.032	0.022	0.027	0.225	0.017
Lu	0.001	0.005	0.001	0.018	0.006	0.004	0.004	0.031	0.003
La	0.001	0.198	0.007	0.302	0.104	0.187	0.711	6.263	0.077
Ce	0.001	0.658	0.026	0.709	0.227	0.407	1.82	13.1	0.243
Pr	0.001	0.111	0.003	0.095	0.026	0.055	0.202	1.50	0.023
Nd	0.001	0.449	0.019	0.437	0.096	0.221	0.792	5.55	0.103
Sm	0.001	0.068	0.009	0.236	0.021	0.057	0.157	1.07	0.028
Eu	0.001	0.028	0.002	0.105	0.004	0.014	0.028	0.255	0.007
Gd	0.001	0.074	0.010	0.344	0.021	0.059	0.135	1.02	0.037

Table 6. Iron and sulfur concentrations for pyrite dissolution experiments at pH = 3.

Sample ID	Sampling time (min.)	Fe (µM)	S (µM)	Molar S/Fe
HY-PASCHKA	60	9.70	6.50	0.670
	480	23.0	27.8	1.21
	1440	54.5	78.2	1.43
HY-PERU4	60	10.2	7.10	0.690
	480	15.8	16.4	1.04
	1440	35.7	48.2	1.35
HY-SPN2A	360	10.1	14.4	1.43
	480	11.5	14.3	1.24
	1440	28.1	42.9	1.53
ILPS-1	60	10.2	7.40	0.720
	480	24.3	25.6	1.05
	1440	59.8	79.9	1.34
INND-1	60	8.60	7.00	0.810
	480	20.2	29.0	1.44
	1440	52.1	84.8	1.63
PAND-1	60	56.1	72.3	1.29
	480	157.0	259.0	1.65
	1440	427.0	828.0	1.94
TXND-3	60	22.2	26.1	1.18
	480	71.4	108.0	1.51
	1440	220.0	400.0	1.82
TXND-4	60	38.3	64.8	1.69
	480	161.0	287.0	1.78
	1440	477.0	807.0	1.69

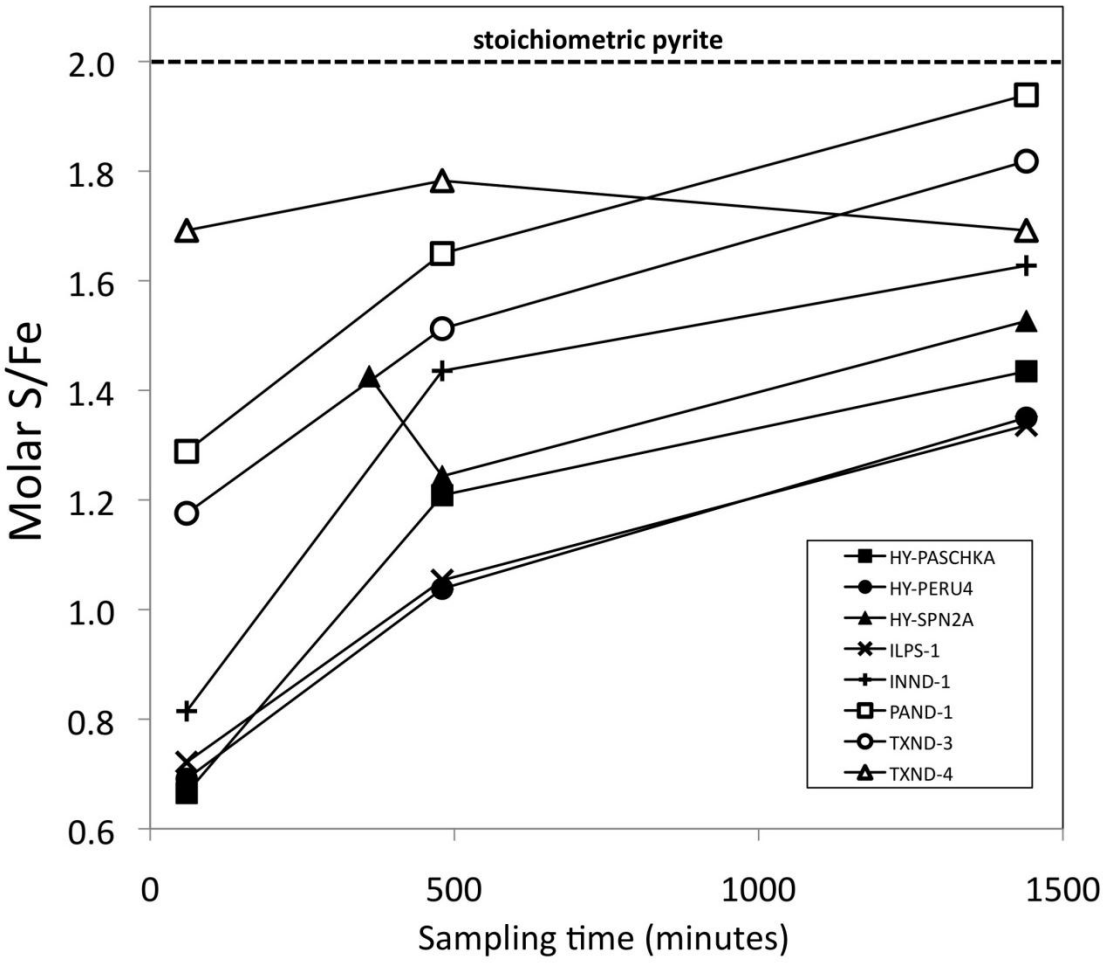

Figure 7. Leachate solution molar S/Fe ratios for each sampling point during the eight pyrite dissolution experiments at pH=3. Note that the bulk solution composition does not reach the stoichiometric pyrite S:Fe ratio (2:1) after 24 hours.

3.3.3 *Isotopic signature: bulk pyrite material*

Iron isotope data for bulk pyrite samples and for leachates from the pyrite dissolution experiments are presented in Table 7 and plotted in Figure 8. Bulk pyrite δ^{56}Fe values, where available, span a range from -0.10 to +1.34. Available δ^{56}Fe values (**Fig. 8**) indicate that the

hydrothermal bulk pyrite samples average a slightly lower value (δ^{56}Fe around 0.0) than do sedimentary pyrite samples (0.5 to 1.3).

Table 7. Iron isotope data for bulk pyrite sample and Fe sample during pyrite oxidative dissolution experiments (relative to standard IRMM – 14).

	δ^{56}Fe				
		Dissolution Experiment Leachates			
Sample	**Bulk Pyrite**	**60 min**	**360 min**	**480 min**	**1440 min**
HY-PASCHKA	0.190	-0.500		-0.150	-0.090
HY-PERU4	-0.100	-0.130		-0.360	-0.630
HY-SPN2A			0.730	0.610	0.600
ILPS-1	1.34	1.21		1.18	1.15
INND-1				-0.380	0.530
PAND-1	0.510	0.570		0.500	0.560
TXND-3		0.740		0.600	0.460
TXND-4	0.570	0.330		0.540	-0.480

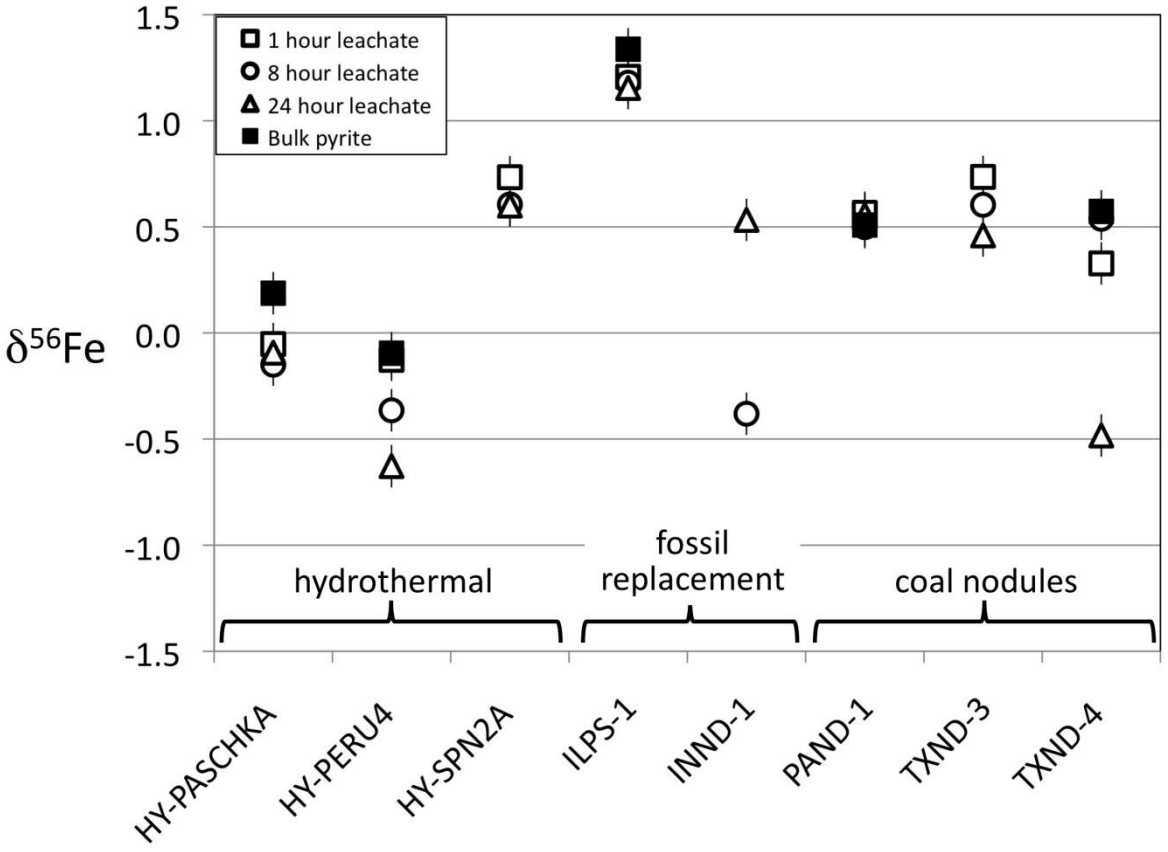

Figure 8. Variation in bulk pyrite (closed square) and pyrite leachate (open symbol) δ^{56}Fe values. Bulk pyrite values are not available for HY-SPN2A, INND-1 and TXND-3.

3.3.4 *Iron isotopes in leachates*

The iron isotope composition of hydrothermal and sedimentary pyrite dissolution samples over the experiment period is given in **Table 7** and plotted against sampling time in **Figure 9**. For those cases where data are available for both the bulk pyrite and leachate samples, the leachates are generally lighter (lower in δ^{56}Fe) than the bulk pyrite value by up to ~1 δ unit (TXND-4; **Figs. 8, 9**). In **Figure 10**, the δ^{56}Fe of leachates are normalized to the first leachate value and plotted against the sampling time for the oxidative dissolution experiments. Generally, the leachate values remain constant or decrease with increasing time of leaching. The major

exception to this is sedimentary pyrite sample INND-1, which shows a significant increase (0.91 δ units) from 480 minutes (8 hours) to 1440 minutes (24 hours). δ^{56}Fe values from the 60 minute leachate and bulk pyrite are unavailable for this sample. In addition, coal pyrite sample TXND-4 shows an increase of ~0.2 δ units from 1 to 8 hours, followed by a precipitous drop by the 24 hour sampling (Fig. 10).

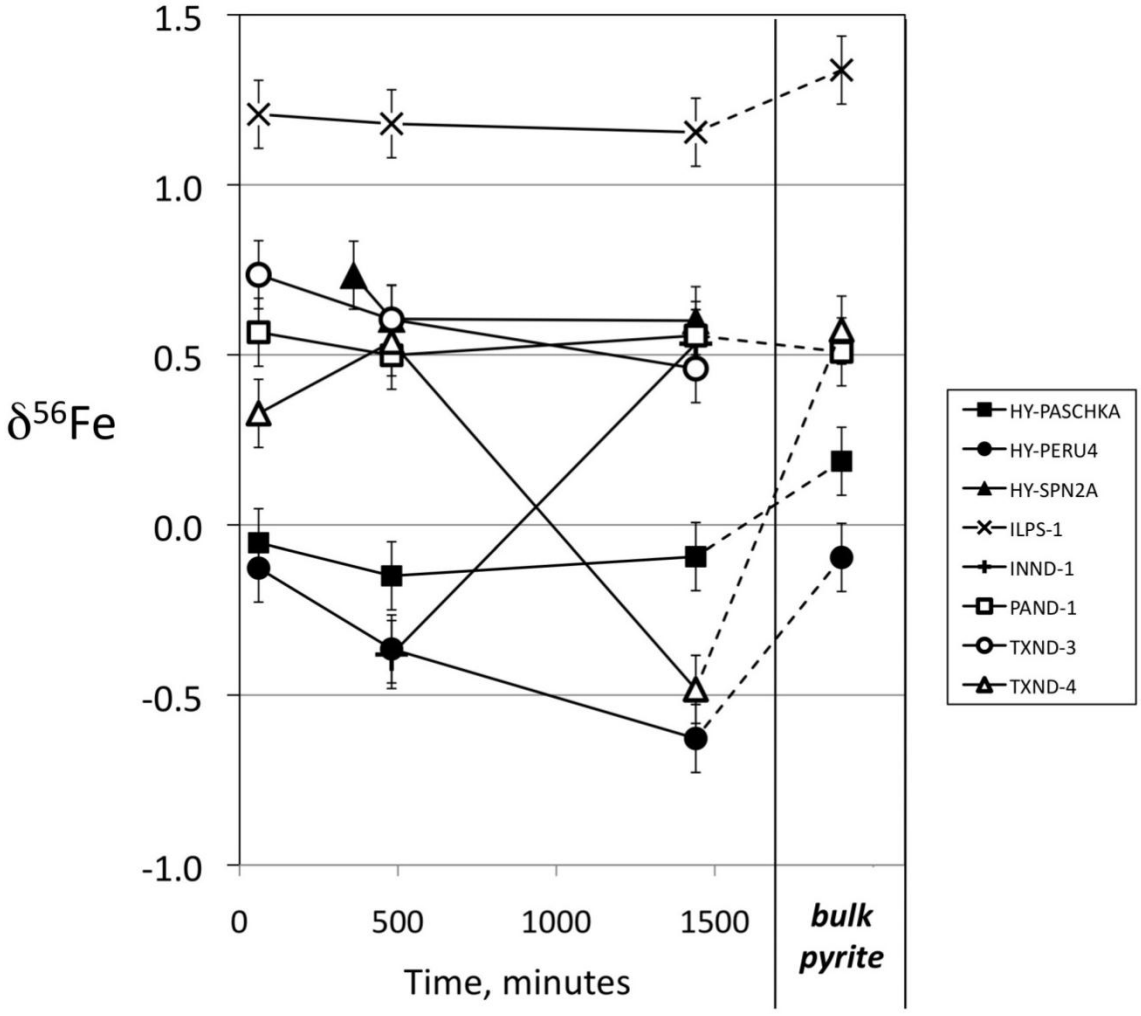

Figure 9. δ^{56}Fe of leachate solution sampled at different time intervals during pyrite oxidative dissolution experiments at pH=3. Where available, bulk pyrite values are plotted on the right. Complete dissolution of the samples would bring the solution to the bulk pyrite δ^{56}Fe value.

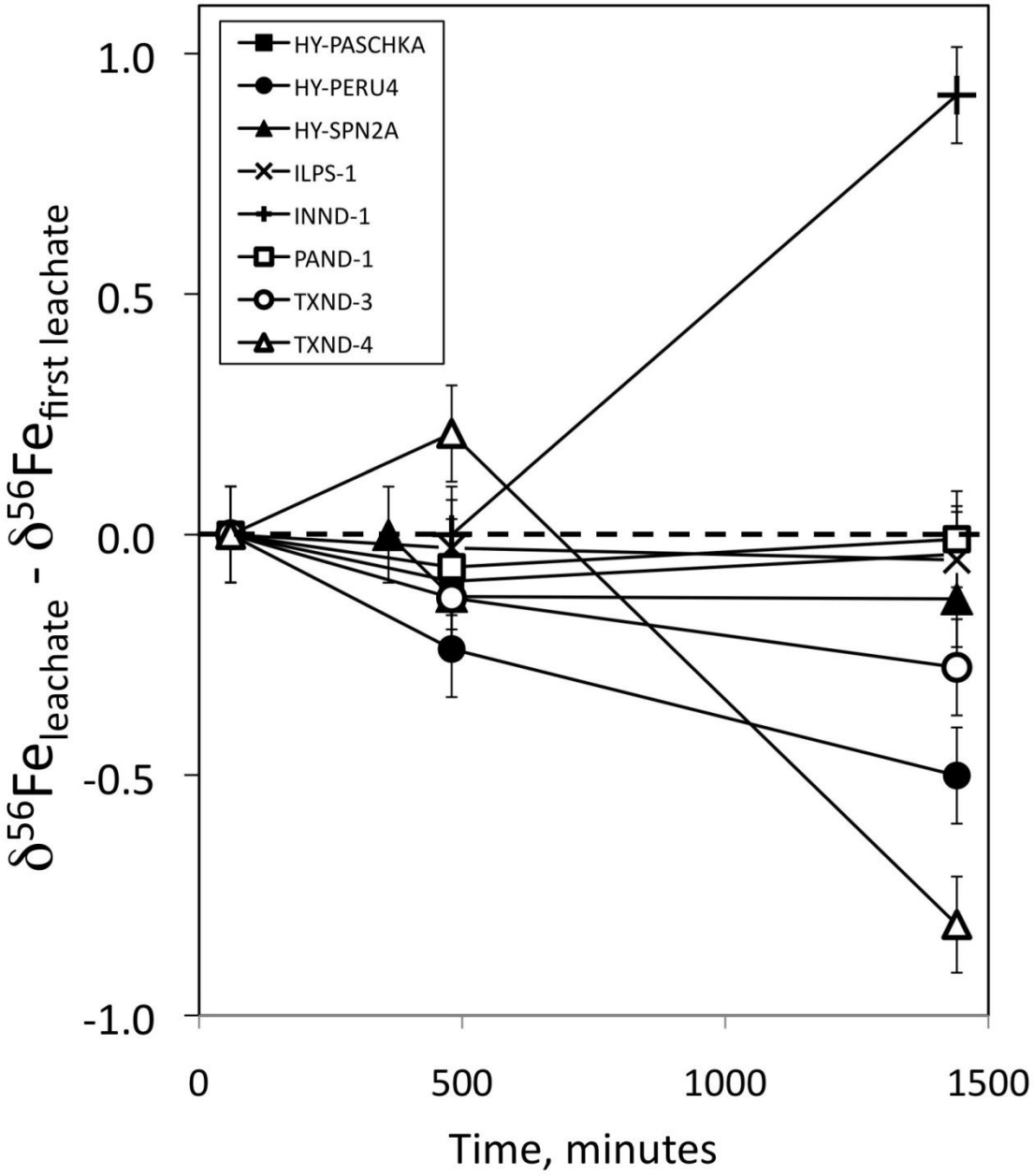

Figure 10. Leachate Fe isotopic evolution for pH=3 experiments is shown as the difference between a given leachate δ^{56}Fe and that of the first leachate (usually at 60 min) for that sample. For sample HY-SPN2A, the first leachate analyzed was at 6 hours, and for INND-1, the first analysis was at 8 hours. In most cases, the leachate δ^{56}Fe remains the same or decreases over time; INND-1 is the major exception.

3.4 DISCUSSION

3.4.1 *Iron isotope composition of bulk pyrite samples*

The rate and extent to which pyrite forms and accumulates within the environment is principally controlled by the amount of organic matter, the availability of reactive iron minerals within the sediment, and the availability of dissolved sulfate. The iron isotope signature of pyrite depends on the fractionation between dissolved precursors and the reservoirs from which the iron is taken. **Figure 11** summarizes the Fe isotopic compositions of pyrite that have been measured to date. Rouxel et al. (2005) (Rouxel et al., 2005) analyzed the Fe isotope composition of diagenetic pyrite from marine shales and found systematic variations in the δ^{56}Fe range and values over geologic time, with highly negative values (some below -3.5‰) occurring mostly in the Archean (pre-2.3 Ga), positive values up to +1.2 in the Paleoproterozoic (2.3-1.8 Ga), and a fairly narrow range of values (-0.5 to +0.2) from ~1.5 Ga to the present (**Fig. 11**). They interpret the pyrite as largely recording the Fe isotope composition of seawater, which was controlled by precipitation of iron oxides (with high δ^{56}Fe) under varying redox conditions and seawater Fe concentrations. In contrast, Archer and Vance (Archer and Vance, 2006) suggest that multiple cycles of dissimilatory iron reduction (DIR) is responsible for a wide range of negative δ^{56}Fe values (-2.7 to –0.9; Fig. 11) that they measured within a small section of core from the Archean Belingwe sedimentary basin in Zimbabwe. Nishizawa et al. (Nishizawa et al., 2010) analyzed numerous Precambrian sedimentary pyrite grains by laser ablation, and found a wide range of δ^{56}Fe values for pre-2.2 Ga sediments (-2.9 to +2.2), while 0.7-0.63 Ga sediments yielded a smaller range of values (-0.2 to +0.6). Pyrite from Phanerozoic and modern sediments yield

mostly negative δ^{56}Fe values (-1.21 to +0.06; (Duan et al., 2010; Fehr et al., 2010; Matthews et al., 2004; Severmann et al., 2006; Severmann et al., 2008). Iron isotope measurements of mid-ocean ridge hydrothermal sulfides and altered oceanic crust yield a range of values from 0.0 to -2.1 (Sharma et al., 2001; Rouxel et al., 2003; Rouxel et al., 2004), and δ^{56}Fe values from a laser ablation study of pyrite from a porphyry Cu-Au deposit ranged from -1.7 to +1.1 (Graham et al., 2004).

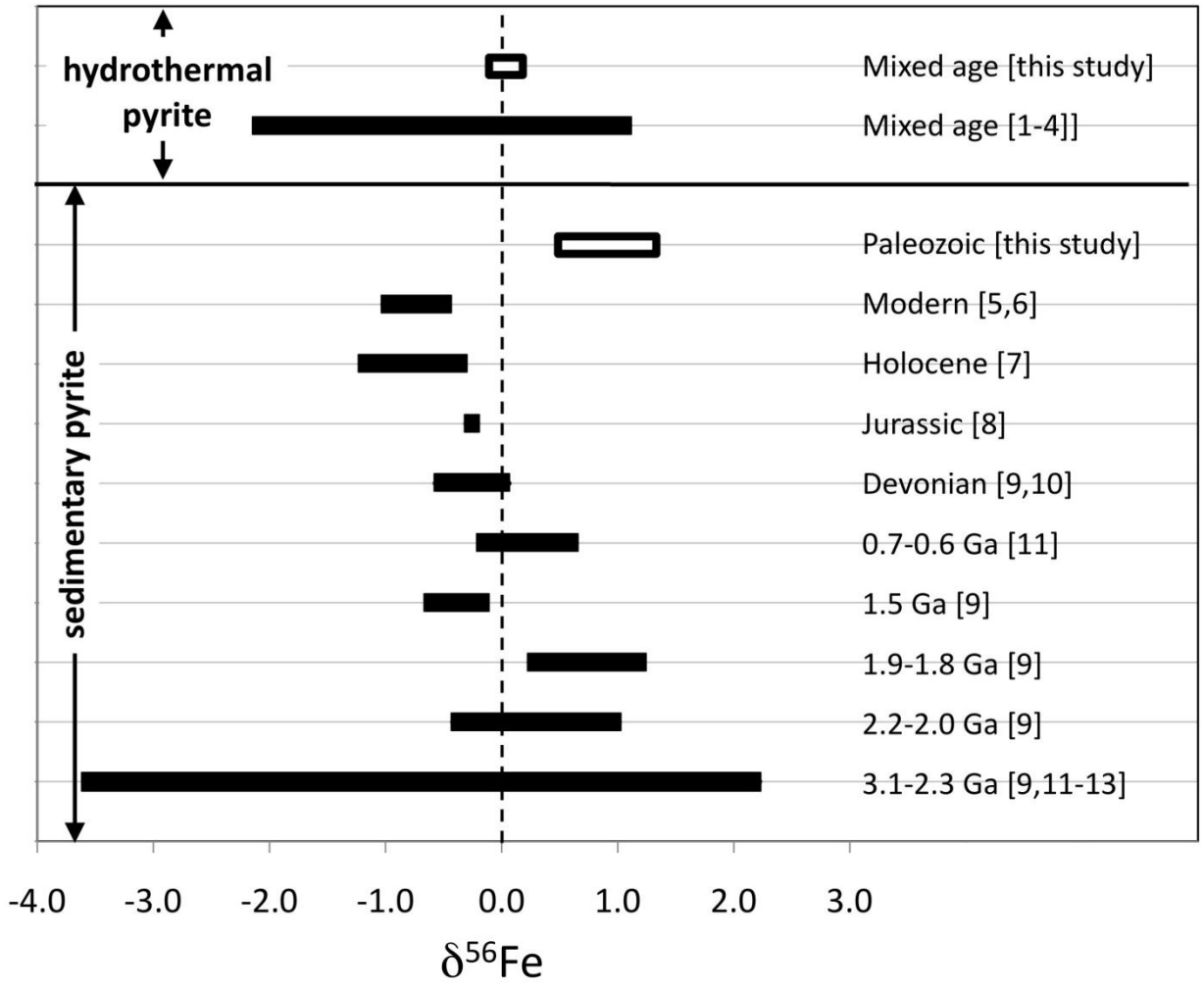

Figure 11. Summary of published Fe isotope data from pyrite of sedimentary and hydrothermal origin, with a comparison to values from this study. Note that we report the only Phanerozoic sedimentary pyrite with significantly positive δ^{56}Fe values.

Figure 11, continued. References cited are as follows: [1] Sharma et al., 2001; [2] Rouxel et al, 2003; [3] Rouxel et al., 2004; [4] Graham et al., 2004; [5] Severmann et al., 2006; [6] Severmann et al., 2008; [7] Fehr et al., 2008; [8] Matthews et al., 2004; [9] Rouxel et al., 2005; [10] Duan et al., 2010; [11] Nishizawa et al., 2010; [12] Johnson et al., 2003; [13] Archer and Vance, 2006.

The δ^{56}Fe values for bulk hydrothermal pyrite from this study (**Fig. 11**) fall within the previously measured range for hydrothermal pyrite (Graham et al., 2004; Rouxel et al., 2003; Rouxel et al., 2004; Sharma et al., 2001). The sedimentary and coal nodule bulk pyrite samples analyzed here, all of Paleozoic age, yield positive δ^{56}Fe values that fall outside of the range of Phanerozoic or modern sedimentary pyrite samples measured to date. These sedimentary pyrite samples are likely to have formed in sediments of non-marine or marginal-marine origin (i.e., continental margin coal-forming mires). The most reactive iron fractions, defined as that fraction of iron in sediments that readily reacts with sulfide during pyrite formation (Canfield, 1989; Canfield et al., 1992), are fine-grained ferric oxides formed via continental weathering, whereas less reactive fractions include clay-bound iron and other iron-containing minerals (Berner, 1984). Other sources of iron may include iron in ionic solution, iron as organic complexes, and iron released by decay of plant debris (Wiese, 1986). Canfield (1989) determined that early pyrite forms almost exclusively from iron oxides, with little evidence for the involvement of silicate minerals. Furthermore, iron oxide reactivity appeared mineral specific, with ferrihydrite and lepidocrocite more reactive towards sulfide than hematite and goethite. Precipitation of Fe(III) oxides enriches the oxides in heavy Fe, so Fe oxides likely provide a high- δ^{56}Fe pool of iron from which the pyrite can precipitate. The iron isotope composition of pyrite in these coal samples does not appear to have been significantly affected by the marine Fe reservoir.

The positive δ^{56}Fe values measured here in coal pyrite contrast with the generally negative shale pyrite values measured in Phanerozoic marine sediments. This suggests that Fe isotopes have the potential to serve as tracers to identify the source of iron in acid mine drainage

situations; that is, to distinguish between pyrite in coal and pyrite from adjacent marine shale units often associated with coal units.

Pyrite from sample ILPS-1 formed as a fossil replacement during diagenesis. The source of iron in the diagenetic fluids could also be dissolved Fe-oxyhydroxides, which would yield a positive δ^{56}Fe value. Although a bulk pyrite δ^{56}Fe value is not available for sample INND-1, the trend of the leachates (**Fig. 8**) suggests that the bulk value could be negative. As discussed below, it is important to consider that bulk sedimentary pyrite samples, possibly including INND-1, could be isotopically heterogeneous (Nishizawa et al., 2010).

3.4.2 *Iron isotope composition of pyrite leachates*

The iron isotope data from these oxidative leaching experiments on pure pyrite separates point to two important observations: (1) δ^{56}Fe values of the leachates tend to fall equal to or below bulk pyrite values, where available (Fig. 8); and (2) with increasing time of leaching, the δ^{56}Fe values tend to stay constant or decrease, with a few exceptions (**Fig. 10**). Fernandez and Borrok (2009) carried out leaching experiments and Fe, Cu and Zn isotope analyses on sulfide-rich rocks associated with hydrothermal metal deposits. These samples, which were crushed and leached in bulk, included mine waste rock and altered volcaniclastic bedrock containing pyrite, chalcopyrite and sphalerite. For experiments conducted at pH=2 (buffered with HCl), they observed a similar trend of decreasing δ^{56}Fe over time, with a drop of ~1 δ unit. A significant difference, however, between their results and ours is that the δ^{56}Fe value in their leachates started out higher than the bulk sample, and gradually approached the bulk sample value. In the experiments reported here, most of the leachate values start out equal to or less than the bulk pyrite value (where available), and decrease with time (**Fig. 12**). Fernandez and Borrok (2009) attribute the trend they observe to dissolution of high-δ^{56}Fe Fe(III) oxides that formed in the

elapsed time between when the rock was crushed and the experiment was started (up to 7 months). In the experiments carried out in this study, great care was taken to remove or minimize any Fe oxides or sulfates from surfaces prior to dissolution (Liu et al., 2008; Paschka and Dzombak, 2004); our Fe isotope results suggest that these surface coatings were successfully removed.

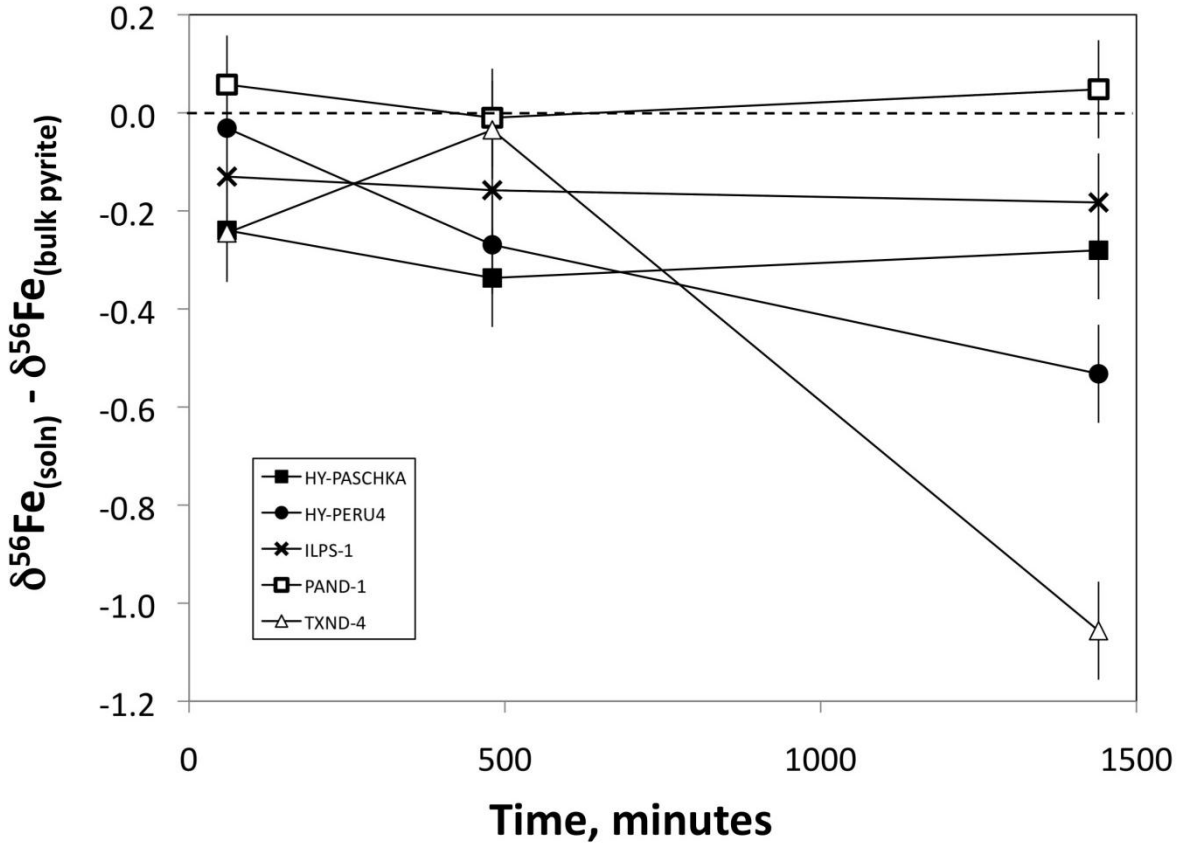

Figure 12. Plot of the difference between the leachate solution δ^{56}Fe values and that of the bulk pyrite for the same sample (where available) from the pH=3 experiments. Note that in most cases the leachate is at or below the bulk pyrite value, which is consistent at least in sign with the expected equilibrium fractionation between aqueous Fe(II) and pyrite.

Theoretical studies by Polyakov and Mineev (2000) and Schauble et al. (2001) suggest that pyrite should be heavier (contain higher δ^{56}Fe) than coexisting aqueous Fe(III). Butler et al. (2005) found measurable isotope fractionation between aqueous Fe(II) and solid FeS (mackinawite) in precipitation experiments; they calculated a kinetic fractionation factor, $\Delta_{Fe(II)-FeS}$ (δ^{56}Fe of Fe(II)[aq] - δ^{56}Fe of FeS[s]), of 0.85±0.30‰, and an equilibrium fractionation factor of ~0.3‰. Thus, in their experiments, the solid FeS was isotopically lighter (lower δ^{56}Fe) than the aqueous Fe(II). Although the formation of mackinawite may be an intermediate step in the formation of pyrite, it is not clear to what extent these experiments can be translated to oxidative dissolution of pyrite.

The data reported in our study do not yield a consistent value for $\Delta_{Fe(II)-FeS2}$, with possible values ranging from 0 to -1. While the direction of fractionation generally agrees with theoretical calculations (Polyakov and Mineev, 2000), there may be other processes controlling the δ^{56}Fe of the pyrite leachates.

Liu et al. (2008) noted that the initial dissolution products from the experiments reported here were enriched in Fe relative to S compared to what would be expected from stoichiometric dissolution of pyrite. They noted that the S:Fe ratio increased with time, but did not reach the 2:1 molar ratio expected for stoichiometric dissolution. When the experiment [S] and [Fe] data are recalculated for the sulfur and iron released during each time interval (i.e., $[S]_{8hrs}$-$[S]_{1hr}$ etc.), it becomes apparent that dissolution ratio may have been approaching that of stoichiometric pyrite. In **Figure 13**, the molar S/Fe ratio for each dissolution time interval is plotted against the % of Fe extracted from the pyrite for all experiments combined. Whether due to selective release of iron (relative to S) or surficial binding of pyrite sulfur, the excess Fe clearly decreases over the course of the experiment. A possible explanation for the decreasing δ^{56}Fe values seen in most of the leachates is that some of the initial excess Fe could have been resorbed on the pyrite

surface as Fe(III), which would be expected to be enriched in heavy iron. Thus, by mass balance, the δ^{56}Fe of the remaining solution would decrease. Fernandez and Borrok (2009) see evidence of Fe(III) in their pH=5 leaching studies of sulfide-rich rocks, but it is not clear that such a process would operate at pH=3. They did not present sulfur concentrations from their leaching experiments to allow complete comparison of the experimental data.

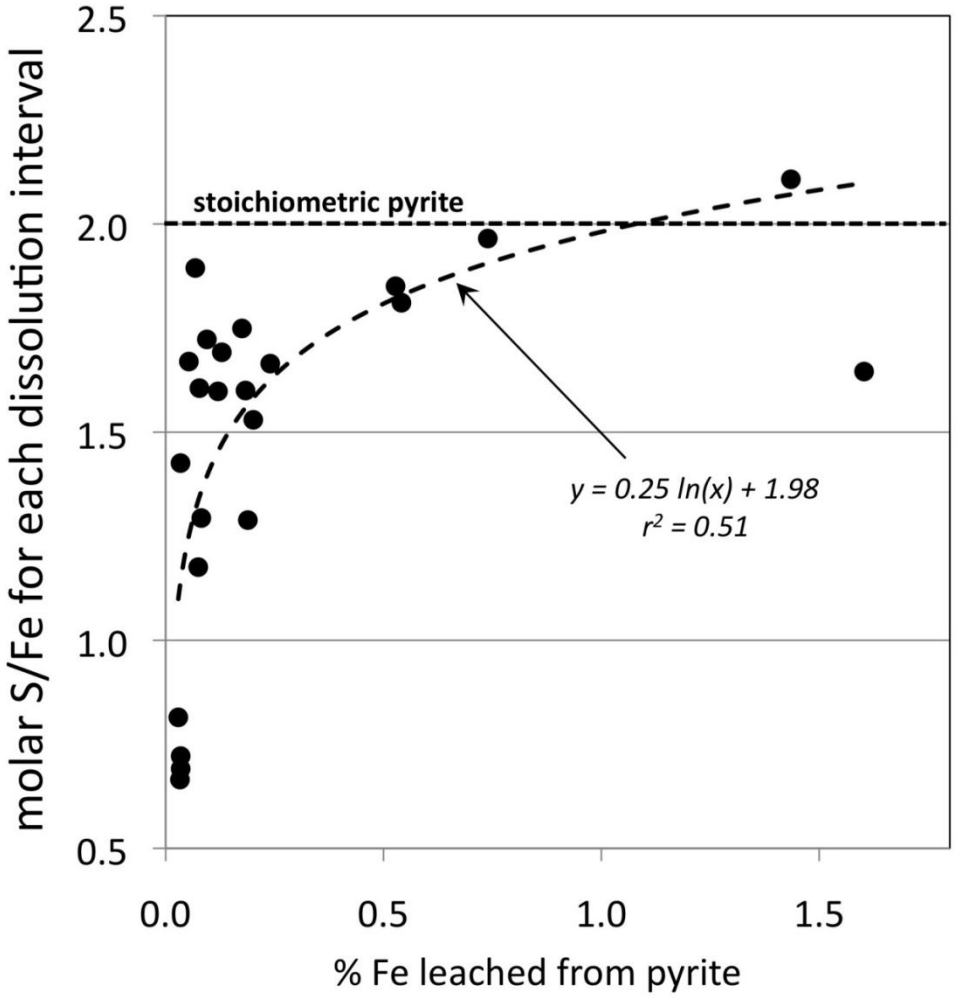

Figure 13. Calculated S/Fe ratio released at each leaching time interval for the pH=3 leaching experiments is plotted against the total amount of pyrite dissolved at the end of that interval. When calculated this way, it can be seen that the Fe and S being released approaches a ratio close to that of stoichiometric pyrite after ~0.5% dissolution (contrast with Fig. 7).

The shifts in δ^{56}Fe of the leachates could also conceivably be caused by isotopic heterogeneity of the pyrite itself. Pyrite in the natural environment is likely to form over long time periods from fluids that could contain multiple sources and generations of iron. This is likely to be especially true in sedimentary pyrite, which forms diagenetically in subsiding basins in which the iron might be expected to evolve continuously over time (e.g., Severmann et al., 2006). While the leachates from both the hydrothermal and the sedimentary pyrite from this study show significant variations in δ^{56}Fe, the largest variations are seen in sedimentary coal sample TXND-4 and fossil replacement INND-1. In particular, INND-1 has a change in δ^{56}Fe of almost 1‰ from 480 to 1440 minutes, and in the opposite direction of most other samples (Figs. 8, 9). This shift could represent a change in dissolution from low- to high- δ^{56}Fe pyrite within the sample, with possible isotopic shifts correlating with morphological changes that affect the ease of dissolution. Recent *in situ* Fe isotope analyses of sedimentary pyrite by laser ablation (Nishizawa et al., 2010) indicate significant shifts in δ^{56}Fe even within individual grains. Similar variations were seen in pyrite from massive sulfide deposits (Graham et al., 2004). Resolution of this issue will require experiments on demonstrably isotopically uniform pyrite, perhaps prepared synthetically under carefully controlled conditions.

3.5 CONCLUSIONS

Oxidative dissolution experiments were carried out on pyrite from multiple petrogenetic environments to investigate possible variations in the iron isotopic composition of pyrite and pyrite leachates. The experimental materials were separated into aliquots of uniform grain size (Wolfe et al., 2007) and were dissolved under carefully controlled conditions (Liu et al., 2008).

A subset of samples from these experiments was analyzed for $^{56}Fe/^{54}Fe$ by multicollector ICP-MS. The primary conclusions from this study are:

- Bulk pyrite $\delta^{56}Fe$ values range from -0.1 to +1.34, with hydrothermal bulk pyrite $\delta^{56}Fe < 0.5$ and coal and sedimentary pyrite nodule $\delta^{56}Fe \geq 0.5$. The hydrothermal pyrite falls within the range of previously measured values, but the coal/sedimentary values are higher than those previously measured for any Phanerozoic sedimentary pyrite. We suggest that this reflects precipitation of pyrite from a high-$\delta^{56}Fe$ continental source, such as Fe derived from dissolution of Fe(III) oxides.

- Leachates from oxidative dissolution of the pyrite at pH=3 tend, with minor exceptions, to yield $\delta^{56}Fe$ values equal to or below those of the coexisting bulk pyrite, by up to ~1‰. This direction of fractionation is consistent with theoretical calculations (Polyakov and Mineev, 2000), but the shifts are not consistent in magnitude.

- The $\delta^{56}Fe$ values of the pyrite leachates decrease with time, again with some exceptions. Suggested explanations for this trend are (1) precipitation of excess Fe as Fe(III) on mineral surfaces over the course of the experiments, driving down the $\delta^{56}Fe$ of the remaining iron; and/or (2) release of iron from different portions of isotopically heterogeneous pyrite grains. It is apparent from this initial study that the Fe isotope approach will have the capability to provide important information about surface processes during oxidative dissolution of sulfides.

- Iron isotopes could be a useful tool in distinguishing between waters that interact with continentally-derived pyrite (e.g., from coal) and pyrite formed under marine conditions. Although the δ^{56}Fe of the leachates were not always equivalent to bulk pyrite values, the spread in bulk values is likely to allow differentiation of iron from these sources. This has implications for quantifying the global sources of Fe into the oceans over geologic time, as well as for understanding and tracking biogeochemical processes that operate in acid mine drainage systems.

4.0 PARTITIONING OF IRON IN ORGANIC AND MINERAL PHASES: SEQUENTIAL EXTRACTIONS OF BITUMINOUS COAL

4.1 INTRODUCTION

Acid mine drainage (AMD) is generated through a series of linked complex geochemical and microbially–mediated reactions that occur when water comes in contact with coal and confining rocks containing the mineral pyrite (FeS_2). This water-rock interaction results in the dissolution of pyrite and associated generation of acidic water with relatively high concentrations of iron and other metals. Sulfides oxidize to release Fe^{2+} and SO_4^{2-}; the subsequent oxidation of Fe^{+2} to Fe^{+3} leads to the production of more acidity and precipitation of Fe oxyhydroxides.

Iron within coal is found almost entirely in the ferrous state (Fe^{2+}); over 90% of the compounds in coal contain Fe^{2+} and the remainder, less than 10%, contain iron as ferric compounds (Fe^{+3}) (**Table 8**) (Badin, 1984). The interaction of iron with both mineral and organic matter makes characterization of iron partitioning difficult. The modes of association of trace elements within the coal matrix and resulting AMD outflows are diverse: they can be absorbed at particle surfaces, be present in the lattice of primary or secondary minerals, or occluded in amorphous material. Heavy and trace metals are partitioned into various phases in sediments, including adsorbed ions, hydroxides, oxides, phosphate, silicates, carbonates, sulfates, sulfides and organometallic complexes (Roychoudhury, 2006). In addition, metal ions are retained on

these solid phases by different mechanisms (ion exchange, outer- and inner-sphere complexation (adsorption), precipitation, or coprecipitation (Filgueiras et al., 2002). These phases are particularly sensitive to surrounding biogeochemical conditions; consequently, mobilization of metals can potentially lead to toxic levels within an aquatic environment (s).

Table 8. Iron species likely to be found in lignite and bituminous coal seams.

Oxidation State	Phase	Formula	Name
2+	Dissolved/adsorbed/ complexed	Fe^{2+}	Ferrous iron
	Solid	$FeCO_3$	Siderite
		FeS_2	Pyrite/Marcasite
		$Fe_{0.8-1}S$	Pyrrhotite
		$\alpha - Fe_2O_3$	Hematite
		Fe(II)-X	Silicates/Clays
3+	Dissolved/adsorbed/ complexed	Fe^{3+}	Ferric iron
	Solid	$Fe(OH)_3$	Ferrihydrite
		$\alpha - FeOOH$	Goethite
		$\beta - FeOOH$	Akageneite
		$\gamma - FeOOH$	Lepidocrocite
Mixed	Solid	Fe_3S_4	Greigite

In order to effectively assess the mobility, availability, and contaminant risk of metals within any given geologic setting impacted by AMD, analytical methods are required not only to determine the total amount of each metal, but also the distribution of phases. Phase-selective extraction techniques are extensively utilized and provide detailed information about the origin, mode of occurrence, biological and physichochemical availability, mobilization and transport of

trace metals and provide a convenient means to determine metals associated in sedimentary deposits (Filgueiras et al., 2002).

The manner in which chemicals partition among dissolved, particulate, and colloidal phases affects both their chemical and physical behavior in different environments. Hence, the goal of extraction methods is to convert the metals bound within these phases into soluble forms with an extractant used at each step (Jiann and Presley, 2002). Several studies (Roychoudhury, 2006) and references therein) have attempted to gain a quantitative understanding of metal portioning within aquatic environments and a number of trace metal extraction techniques were developed using various wash solutions, including strong mineral acids, reducing agents, surfactants, and a variety of organic acids and chelating agents (Bassi et al., 2000). Reagents utilized in single or multi-step extraction schemes are chosen on the basis of their supposed selectivity and specificity toward particular physicochemical forms, although variations in reagent strength, volume and extraction times typically vary (Li et al., 1995). The extractants more commonly used in sequential extraction schemes are generally applied in the following order: unbuffered salts, weak acids, reducing agents, oxidizing agents and strong acids (Rauret, 1998). Many of the sequential extraction schemes employed are based on the five-stage Tessier protocol (Tessier et al. 1979) or a modification thereof (**Table 9**); however, there are virtually no examples of the sequential extraction methodology aimed at determining the distribution of iron within organic rich sediments. The sequential leach procedure presented here is a modified version of the method developed by Poulton and Canfield (Poulton and Canfield, 2005). In addition, to evaluate the reproducibility of this method, ashed samples were spiked with known amounts of goethite, siderite and pyrite. Individual samples of each mineral were also subjected to the same reagents to replicate and confirm the results presented by Poulton and Canfield

(Poulton and Canfield, 2005). Development of a successful iron fractionation technique must take into account the dynamics of dissolution processes and their inhibition, and requires an appreciation of the reactions which describe the transfer of the chemical species between a given mineral, as well as an understanding of the structure and chemical bonding at the mineral-solution interface.

The main objective of this study is to develop an extraction technique to quantify and understand the physico-chemical distribution of iron within organic rich sediments such as coal. Determining the modes of element occurrence may provide information on the depositional conditions and geologic history of coal-bearing sequences and individual coal beds, and in the characterization of mineral matter source area (**Table 10**) (Ward, 2002). Furthermore, environmental problems resulting from coal and coal ash utilization may be predicted or minimized with information on the modes of occurrence of elements, minerals and phases in coal and coal waste products (Vassilev and Vassileva, 1996). The development of a sequential extraction technique that targets specific "model" iron compounds known to occur in coal and combinations of compounds, will confirm and provide more knowledge on the chemical mechanisms taking place during pyrite formation, subsequent dissolution, and generation of AMD, as well as the extent to which the coal matrix affects mineral dissolution. The ability to quantitatively partition iron in coal and organic-rich sediments would not only aid in our understanding of AMD generation, but could also provide important information about iron biogeochemistry and the petrogenesis of Fe-rich phases such as pyrite in modern and ancient sedimentary environments.

Table 9. The relationship between metal mobility in different operationally-defined phases and extractant strength of commonly used chemical reagents in sequential extraction procedures is shown. Compiled from Tessier (1979), Filgueiras et al. (2002), and Gleyzes et al. (2002).

Operationally Defined Fraction	Extractant	"Tessier" Method (Tessier, 1979)
Exchangeable[a]	$CaCl_2$, $MgCl_2$, $BaCl_2$, NH_4Cl, NH_4CH_3COO, $Mg(NO_3)_2$, $Ca(NO_3)_2$, or NH_4NO_3	$MgCl_2$, pH = 7 LSR[*] = 8:1
Acid Soluble[b] *(Carbonates)*	$NaCH_3COO$ (NaOAc), CH_3COOH (HOAc), orEDTA	NaOAc/HOAc, pH = 5 LSR: 8:Residue$_{exchange}$
Easily Reducible[c] *(Mn Oxides)*	HOAc, HNO_3, or $NH_2OH{\bullet}HCl$	$NH_2OH{\bullet}HCl$ in 25% HOAc, pH = ~2 LSR: 20: Residue$_{carb}$
Easily Oxidisable[d] *(Humic & Fulvic Acids)*	NaClO, or $K_4P_2O_7$	—
Moderately Reducible[e] *(Fe oxides, am)*	HOAc, HCl, $NH_4C_2O_4$, $NH_4C_2O_4/H_2C_2O_4$, or NH_4Ox/HOx	*Dissolved Mn oxides and Fe oxides (am) using the same reagent, see above*
Oxidisable[f] *(Oxides, Sulfides)*	H_2O_2, H_2O_2/NH_4OAc, NaClO, $Na_4P_2O_7$, or $K_4P_2O_7$	*Oxidisable*: H_2O_2/HNO_3, pH = ~2
Poorly Reducible Oxides[g] *(POR, Crystalline oxides)*	Na Citrate/$Na_2S_2O_4$, $Na_2S_2O_4$, NH_4Ox/Ascorbic acid	*Poorly Reducible Oxides*: followed by NH_4OAc LSR: 10: Residue$_{EasuktRed}$
Residual[h] *(Silicates)*	HF, HNO_3, $HClO_4$, or a mixture of these	HF - $HClO_4$ LSR: 5: Residue$_{Oxid,POR}$

← ← ← ← Metal Mobility ← ← ← ←

→ → → Leachant Strength → → →

[*] LSR = Liquid (mL): Solid (grams) ratio

[a] *Exchangeable*: includes weakly-sorbed metal species retained on the surface by relatively weak electrostatic interactions and those that can be released by ion-exchange processes

[b] *Acid Soluble*: includes metals that which are precipitated or coprecipitated with carbonate

[c, e, g] *Reducible*: targets dissolution of Mn oxides ([c]), amorphous Fe oxides ([e]), and crystalline Fe oxides ([g]) by controlling the Eh and pH of the extractant.

[d] *Easily Oxidisable*: targets trace metals that are associated with organic matter including living organisms, organic coatings on inorganic particles and biotic detritus

[f] *Oxidisable*: includes organic material that is not considered very mobile or available as well as metals bound to sulfide

[h] *Residual*: Primary and secondary minerals containing metals in their crystalline lattice

Table 10. Coal minerals and their origins (after Speight, 2005)

Mineral Group	Syngenetic Formation (*Intimately Intergrown*)		Epigenetic Formation	
	Transported by Wind or Water	Newly Formed	Deposited in Fissures, Cleats, and Cavities (Coarsely Grown)	Transformation of Syngenetic Minerals (Intimately Intergrown)
Clay Minerals	Kaolinite, illite, sericite, clay minerals with a mixed-layer structure		—	Illite, chlorite
Carbonates	—	Siderite-ankerite concretions, dolomite, calcite, ankerite	Ankerite, calcite, dolomite	
		Siderite, calcite, ankerite in fusite		
Sulfides	—	Pyrite concentrations, coarse pyrite (marcasite), concretions of FeS_2-$CuFeS_2$-ZnS	Pyrite, marcasite, sphalerite (ZnS), galena (PbS), chalcopyrite (CuS)	Pyrite from the transformation of syngenetic $FeCO_3$ concretions
		Pyrite in fusite		
Oxides	—	Hematite	Goethite, lepidocrocite	—
Quartz	Quartz grains	Chalcedony and quartz from the weathering of feldspar and mica	Quartz	
Phosphates	Apatite	Phosphorite	—	—
Heavy minerals, accessory minerals	Zircon, rutile, tourmaline, orthoclase, biotite	—	Chlorides, sulfates, nitrates	—

4.2 METHODS

All reagents were certified A.C.S. or trace metal grade. Milli-Q 18 MΩ water (MQW) was used to make up all extractants, as well as for the water rinse step of the procedure. All HDPE plasticware used for reagent solutions and sample leachates were cleaned with 30% HNO_3 (soaking overnight). The PTFE centrifuge tubes were cleaned using 50% HCl → 50% HNO3 → 50% HCl (eight hours for each step), followed by rinsing in MQW.

4.2.1 *Samples*

The sequential extraction procedure developed in this study was tested on bituminous coal samples (**Table 11**). Samples were selected to reflect a range of thermal maturity, ash percentage and sulfur content.

Synthetic goethite was prepared according to the standard methods of Cornell and Schwertmann (1996). A volume of 180 mL of 5M KOH was added to 200 mL of 1 M $Fe(NO_3)_3$. The resulting suspension was diluted and heated at 70°C for 60 hours in a drying oven. X-ray diffraction analysis (Philips XRD PW3710; Almelo, Netherlands) confirmed that the sample was goethite. Siderite nodules were collected from Kossuth (Clarion County), PA (41°16'40.79"N, 79°33'24.76"W) and crushed into pea-size pieces using a sledgehammer. The sledgehammer, steel plate and sample were wrapped in aluminum foil to prevent iron contamination. The siderite sample was transferred to a tungsten carbide cylinder and milled into a powder for approximately 5 minutes using a Spex SamplePrep 8000 series mixer mill. Approximately 5-6

grams of material were transferred to a brass sieve set (75 μm mesh was used) and shaken for 10 minutes in a sieve shaker. Powder <75 μm was collected for experimental work. Hydrothermal and sedimentary pyrite samples were collected and prepared according to the wet sieving method described in Wolfe et al. (2007). X-ray diffraction analysis indicates that the samples were pyrite. Additional aliquots (~0.1 g) of pyrite powder were completely dissolved in 10 mL concentrated nitric acid and further diluted to 5% nitric acid for iron and sulfur analysis by SpectroFlame EOP ICP-AES (Kleve, Germany) using EPA Method SW 846 Accuracy of measurements are within ± 5% of true values. The results (**Table 12**) indicate that the samples consist of stoichiometric FeS_2.

Table 11. Geographic location, proximate and ultimate analysis of two bituminous coal samples used in this study. Sample CL-TC-CL1 was collected by the author, and used in ASE extraction experiments. DECS-24, provided by the Penn State Coal Sample Bank, was subjected to lower temperature ashing following by a chemical sequential leach.

	CL-TC-CL1	**DECS-24**
Coal Seam	Clarion	Illinois #6 (Herrin)
ASTM Coal Rank[a]	—	hvCb[b]
Sample Type	Grab	Channel - Seam
State	PA	IL
County	Clarion	Macoupin
Ash %, dry	7.42	13.4
Sulfur %, dry	—	5.53
Mineral Matter %, calc[c]	~9.00	16.4

[a] ASTM coal rank is determined on the basis of its calorific value, on a moist, ash-free basis.

[b] hvCb = high volatile C bituminous coal, calorific value ranges between 11,500 – 13,000 btu

[c] Calculated using the Parr formula; MM (%) = (1.08 * Ash %) + (0.550 * Sulfur, %), where MM is mineral matter. No sulfur data were available for CL-TC-CL1, so the sulfur value of a Lower Kittaning coal sample (PSOC-1516, PSU Coal Bank Database) was substituted into the equation (1.40%). The Lower Kittaning coal seam is above the Clarion coal seam, thus the sulfur value of the CL – TC – CL1 should be equal to or greater than the Lower Kittaning coal seam given similar depositional environments.

Table 12. Mineral samples used in the study. [a]HY-QUBC1 was purchased at the Carnegie Museum of Natural History Rock and Mineral Show (2004). Composition was determined using x-ray diffraction and chemical analysis. A chemical analysis of HY-QUBC1 was not conducted; however, sample TXND-4 had a molar ratio of approximately 2:1, indicating insignificant contribution from other elemental species.

Sample ID	Source	Morphology	Petrogenetic Environment	Mineralogy
GOE 1	Synthetic	—	—	Goethite
SID – 1	Kossuth, PA	Nodule	Sedimentary	—
HY – QUBC1	CMNH[a]	Euhedral cube	Hydrothermal	Pyrite with minor quartz
TXND – 4	Texas	Nodular	Sedimentary, within coal	Pyrite

4.2.2 *Iron Extractions – Overview*

All iron extractions were performed under oxic conditions. Extractions were performed using the reagents given in Table 13. Surficially-bound (Fe_{suf}) and organically-bound (Fe_{org}) iron were removed using a Dionex Accelerated Solvent Extraction System (ASE 100, Dionex, California, USA). The instrument operation parameters used to optimize extraction for the Fe_{surf} and Fe_{org} fractions can be found in **Table 13**. After ashing, each sample was subjected to a sequential extraction leach to collect iron fractions from mineral matter. The sequential leach procedure is a slightly modified version of the method developed by Poulton and Canfield (2005). The extractions were performed under oxic conditions in constantly agitated in acid-cleaned 50 mL HDPE (high-density polyethylene) centrifuge tubes. The extractant volume was 20 ml except where otherwise noted. Sediment extractions were performed with a sample size of approximately 200 mg.

Table 13. Details of the developed extraction scheme with target phases and reagents. The extraction scheme is a combined accelerated solvent extraction procedure and sequential chemical leach method.

	Terminology	Target Phase	Extraction
ASE Extraction	Fe_{surf}	Weakly sorbed iron retained on the coal surface; can be released by ion-exchange processes	1 mM EDTA solution, followed by acetone rinse
	Fe_{org}	Fe organically bound to the macromolecular coal structure	Undiluted 1-Methyl-2-pyrrolidinone, followed by acetone rinse
Chemical Sequential Extraction	Fe_{carb}	Carbonate Fe: including siderite and ankerite	0.3 M $NaCH_3COO$ buffered with acetic acid, pH = 4.56
	Fe_{oxides}	Oxide Fe: ferrihydrite, lepidocrocite, goethite	0.3 M $Na_2S_2O_4$ buffered with 0.15M Na Citrate/0.10M $NaHCO_3$. Fluxed at 80°C for 24 hours. Ultrasonicated for 2 hr at 70°C
	Fe_{pyr}	Pyrite	Conc. HNO_3. Fluxed at 80°C overnight.

Table 14. ASE instrument parameters.

Instrument: Method Control			This study
Parameter	**Function**	**Value Range**	**Experimental Parameter**
TEMP	Temperature at which to heat the extraction cell.	Off, 40 to 200°C	50°C
STATIC TEMP	Static solvent extraction time.	0 – 99 min	15 min
FLUSH VOLUME	The amount of solvent to flush through the extraction cell after the static heating step. This parameter is expressed as a percentage of the cell volume.	0 to 150% volume in 5% increments	100%
PURGE VOLUME	The amount of time the cell is purged with nitrogen.	20 to 900 sec	100 sec
STATIC CYCLE	The number of times the static and flushing steps are performed. When more than one cycle is specified the flush volume is divided among the cycles.	1 to 5	2

In addition, twelve replicates, (three each of siderite, goethite, pyrite, and a mineral mix of known quantities of siderite, goethite and pyrite), were carried out to evaluate the reliability of the mineral extraction procedure. The percent recovery of the sequential extraction procedure for iron was calculated by summing the iron yield from each fraction and dividing by the total metal concentration calculated from ICP data.

Total Fe was determined by leaching ashed coal samples (ashed at 800°C) with concentrated HCl. Each sample was centrifuged for 15 minutes at 1200 rpm and the leachate decanted into acid cleaned PMP beakers. Solutions were evaporated to dryness and brought up in 2% HNO_3 to analyze for iron and sulfur concentration using ICP-AES (G and C Coal Analysis Lab, Inc.; Summerville, PA).

4.2.3 *Iron Extractions – Detailed procedure*

Step 1: Exchangeable surface species

A 10 mL ASE 100 stainless steel extraction cell was filled with a mixture (3:1 v/v) of coal sample and Teflon (PTFE) beads (3 mm, Chemware) and subjected to extractions using ethylenediaminetetraacetic acid (EDTA). To extract surficially-bound Fe, a 1.13 mM EDTA solution was prepared daily by adding 0.331 g of EDTA salt (99%, Acros Organics) to 1500 mL of ultra-high purity water (MQW). Solutions were prepared in an acid cleaned Dionex 2-L borosilicate glass solvent bottle. The extraction cell was purged with nitrogen gas for 100 seconds, and flushed with the 5 mL of EDTA solution for 8 minutes at 40°C. This cycle was repeated two more times, for a total of three cycles. At the conclusion of the run, the EDTA solution was collected in acid rinsed 250 mL glass bottles fitted with solvent-resistant septa (TFE coated on solvent side) vial lids. The bottle was purged with nitrogen prior to removal from the unit. To remove EDTA from the coal surface prior to step 2, the extraction cell was purged with nitrogen gas for 100 seconds, and flushed with the 5 mL of acetone (Optima, Fisher Scientific) for 8 minutes at 40°C. This cycle was repeated two more times, for a total of three cycles, to verify that exchangeable iron was quantitatively removed during the first extraction. The acetone solution was collected in acid rinsed 250 mL glass bottles. Each experiment was repeated in triplicate. The EDTA and acetone solutions were transferred to acid cleaned PMP beakers and evaporated overnight to dryness. A 30% HCl solution was added to the solid residue to dissolve iron and allowed to flux overnight on a hot plate at 80°C. The samples were transferred to 15 mL acid rinsed test tubes and centrifuged for 5 minutes at 3000 rpm. Solutions were decanted into 30

mL Teflon vials and evaporated to dryness overnight at 150°C. Post evaporation, the iron pellet was dissolved in 2% HNO_3 for iron analysis using a SpectroFlame EOP ICP-AES (Kleve,Germany).

Step 2: Organically bound species

To extract organically-bound Fe, undiluted 1-Methyl-2-pyrrolidinone (NMP, 99%, Acros Organics) was transferred to an acid –cleaned Dionex 2-L borosilicate glass solvent bottle. The solvent bottle was covered with aluminum foil to prevent solution decomposition. The extraction cell was purged with nitrogen gas for 100 seconds, and flushed with the 5 mL of NMP solution for 8 minutes at 40°C. At the conclusion of the run, the bottle was purged with nitrogen and the NMP solution was collected in an acid rinsed 250 mL glass bottle and transferred to acid rinsed PMP beakers. ASE extraction solutions were evaporated almost to dryness in PMP-beakers, transferred to acid-cleaned ceramic crucibles, covered with ceramic lids, and ashed at 800°C for 4 hours. The ashed samples were leached using concentrated HCl, evaporated to dryness and brought up in 2% HNO_3 to analyze for iron concentrations by ICP-AES.

Step 3: Removal of carbon matrix.

The solid residue was collected from the extraction cell, transferred to an acid-cleaned quartz crucible and subjected to low temperature ashing (LTA, Steel et al., 2001). Samples were placed in a preheated (200°C) in a muffle furnace. The temperature was raised to 350°C over a period of 24 hours. After the second day of ashing at 350°C, the coal was ground using a ceramic pestle to expose encapsulated carbon. Crucibles were rotated in the furnace throughout ashing to

provide homogeneity. The coal was considered to be fully ashed when the weight of the sample remained unchanged by less than 1%. This occurred in 3-5 days.

Step 4: Carbonates

After ashing, the crucible contents were transferred to acid cleaned 50 mL test tubes. Approximately 15 mL of a 1M sodium acetate solution (NaOAc, prepared daily), buffered to pH 4.5 with concentrated glacial acetic acid, was added to each test tube. The test tubes fluxed for 48 hours in a heated water bath (50°C). Solutions were centrifuged for 10 minutes at 1200 rpm and the solution was decanted into acid cleaned PMP beakers. The solid residue was rinsed with 10 mL MQW, centrifuged for 10 minutes at 1200 rpm, and the solution was decanted into the appropriate PMP sample beaker. Samples were evaporated to dryness on a hot plate at 100°C overnight. The evaporated residue was dissolved in 50% HNO_3; 4.8 mL of the nitric solution was transferred to a 15 mL HDPE bottle and diluted to 15 mL with MQW for iron and sulfate concentration analysis.

Step 5. Oxides

A 0.3M sodium dithionite solution, buffered to pH 4.5 with 0.3M sodium citrate/0.1M sodium bicarbonate, was tested for iron oxide extraction. The buffer solution was prepared by was prepared by adding 44.6 g of sodium citrate salt ($Na_3C_6H_5 \bullet 2H_2O$), and 4.9 g sodium bicarbonate ($NaHCO_3$) to 0.50 L MQW. 15 mL of buffer solution was added to the remaining solid from step 4. Approximately 0.3g of sodium dithionite salt ($Na_2S_2O_4$) was added to each test tube, and the tubes were placed in a water bath to flux at 80°C overnight. An additional 5 mL of buffer solution, and 0.3 g of sodium dithionite, was added to each test tube the following

morning. The final concentration of sodium dithionite for each sample was approximately 0.3M. Following the second addition of sodium dithionite salt, the samples were placed in a 75°C water bath and ultrasonicated for 35 minutes. All oxides appeared to be in solution, based on a visual inspection of tube contents. The samples were centrifuged at 1200 rpm for 15 minutes. The solutions were decanted into acid rinsed PMP beakers. The remaining solid residue was rinsed with 5 mL fresh sodium citrate/bicarbonate solution and centrifuged for 15 min at 1200 rpm and the solution decanted into the appropriate sample beaker. To remove the buffer solution from the reside, 5 mL MQW was added to each sample. The samples were centrifuged for 15 minutes at 1200 rpm and the solution decanted into the appropriate sample beaker. Solutions were evaporated to dryness. 15 mL of 50% HNO_3 was added to each beaker and the solution gently shaken until the contents dissolved. The solution was transferred to 15 mL acid cleaned test tubes and centrifuged for 10 minutes at 4000 rpm. 5 mL of each sample was transferred to an acid cleaned HDPE bottle and the total volume brought to 10 mL with 18.2 MΩ water.

Step 6. Sulfides

A volume of 15 mL of concentrated nitric acid was added to the solid remaining after Step 5 to dissolve metal sulfides. The samples were fluxed overnight in a water bath at 80°C and centrifuged for 15 minutes at 1200 rpm the following morning. 5 mL of each sample was transferred to an acid cleaned HDPE bottle and the total volume brought to 10 mL with MQW.

4.3 RESULTS

In order to determine how effective the method was for extracting iron from different iron-bearing phases, a total percent recovery value was calculated: the total concentration obtained from bulk analysis for a given sample was compared to the total concentration extracted by the method. Table 15 shows the weight % Fe extracted from coal sample CL-TC-CL1 using the ASE methodology, compared to total iron content. The ash content of this sample (n=3) was 7.42%. Measured iron content (ICP-AES) of these samples ranged between 2.20 and 2.76 mg/g. **Table 16** shows the weight % Fe extracted from each sample chemical extraction, compared to total iron content. In order to assess the overall accuracy of this method, the sum of the iron concentrations from each extraction step were compared with the calculated values of concentration. Significant features of these data are:

a) All iron is quantitatively leached from the ashed, unspiked coal sample (DECS-24A and -24B); the average Fe yield is approximately 100% (n = 2).

b) The selected extractants failed to quantitatively dissolve iron within the spiked ash samples, mixed mineral sample, and single mineral separates. Specifically:

    a. Sodium acetate was marginally successful in dissolving siderite (34.30%).

    b. None of the samples containing goethite were appreciably soluble using sodium dithionite buffered with sodium citrate/sodium bicarbonate.

    c. Concentrated nitric acid was ineffective in dissolving samples containing known amounts of pyrite; however, sodium acetate was effective in dissolving pyrite (61.58%).

Table 15. Calculated concentration of iron in coal sample CL-TC-CL1 based on analyzed Fe concentrations.

	[Fe] conc, *mg/L*	% error	[Fe], *mg/g*		% Yield, Fe
EDTA 1	404.2	1.753	2.623		71.46
Acetone, Rinse 1	5.860	2.965	0.0070		0.9990
				→	**72.46%**
EDTA 2	44.51	0.9650	0.2600		7.292
Acetone, Rinse 2	7.350	3.291	0.0430		1.202
				→	**8.494%**
EDTA 3	83.90	1.655	0.4940		13.84
Acetone, Rinse 3	13.85	3.134	0.0740		2.079
				→	**15.92%**
			Total EDTA extracted - Fe		**96.87%**
NMP 1	27.27	1.127	0.1680		4.716
			Total NMP extracted - Fe		**4.716**%
			Total Fe extracted (EDTA + NMP)		**101.59%**

Table 16. A comparison of the amounts of iron removed by different extraction reagents.

		Iron Extracted (wt. %)			
	Sample	**NaOAc**	**$Na_2S_2O_4$**	**HNO_3**	**Total**
	DECS 24A	64.58	2.970	8.830	103.4
	DECS 24B	73.45	3.688	6.787	96.59
Mineral Spike	DECS 24 + Goe	0.4984	0.2239	1.844	2.566
	DECS 24 + Sid	*ND*	4.531	3.139	*(7.670, n = 2)*
	DECS 24 + Pyr	61.58	1.049	8.671	71.3
Minerals	Siderite	34.30	0.6581	0.1824	35.14
	Goethite	0.3836	0.3143	0.0634	0.761
	Pyrite	*ND*	0.1724	*ND*	*(0.1724, n = 2)*
	Goe + Sid + Pyr	*ND*	3.273	2.529	*(5.802, n = 2)*

4.4 DISCUSSION

The method developed here attempts to quantify iron partitioning in coal by first removing exchangeable and organically-bound Fe using an accelerated solvent extraction method. Solid residue remaining in the extraction cell following Step 2 is then ashed at low temperature (Steel et al., 2001) and followed by four chemical extraction steps. These two method components were evaluated independently, operating on the rationale that if each method was successful independently, then when combined, the entire method would prove successful.

4.4.1 *ASE Extractions*

Coal structure is a three dimensionally cross-linked macromolecular system possessing aromatic and hydroaromatic ring structures joined by hydrogen bonds and covalent linkages consisting of short chains of carbon, oxygen, sulfur or nitrogen atoms (Assis et al., 2000). The advantages of using the ASE instrument for iron extraction are fourfold: 1) increased temperatures disrupt non-covalent solute-matrix and solute-solute interaction; 2) increased temperatures decrease solvent viscosity and surface tension, allowing for better matrix penetration and wetting; 3) higher pressures allow for better solvent penetration into the matrix relative to atmospheric pressure; and 4) increased pressure aids in the solubilization of air bubbles so that the solvent more rapidly comes in close contact with the entire sample matrix. ASE methodology is predominantly used to investigate the molecular structure of coal and, to date, no studies have used this instrument to determine metal association with the coal matrix.

The ASE instrument method extracted almost 100% of the total iron from coal sample CL-TC-CL1 (Table 15). Over 90% of iron was removed using 1.13 mM EDTA solution; however, it is currently unknown to what extent EDTA will dissolve individual mineral grains. Raiswell et al. (Raiswell et al., 1994) demonstrate that the amount of iron leached does not change during leaching experiments unless grain sizes are <63 μm. The amount of iron released increased rapidly through the 43-63 μm, 20-43 μm and <20 μm fractions. While the grain size distribution of iron bearing minerals within the coal sample were not measured in this study, it is feasible that EDTA could leach iron from mineral surfaces, thus biasing iron results. This hypothesis is supported by experimental work by Kirpichtchikova and coworkers (Kirpichtchikova et al., 2006). The authors report that equilibrium thermodynamic calculations

for minerals containing multivalent cations, such as Fe^{3+}, completely dissolve below pH 9 when in contact with 1% excess EDTA. However, they found that the concentration of multivalent cations increased with successive rinses, which contradict the results obtained from this experiment.

1-Methyl-2-pyrrolidinone (NMP) was selected as an appropriate solvent because of its unique ability to dissolve both polar and non-polar substances within coal and, due to this property, is considered a "super solvent." The purpose of this solvent is to separate the carbonaceous material from the inorganic portion within coal, effectively removing all inorganic matter from the coal sample. The soluble portions of coal are typically carbonaceous aromatic macromolecules trapped within the 3-dimensional cross linked lattice of coal. The product of the solvent extraction (coal extract) is a solid carbonaceous material thought to have almost no ash (Stoffa, 2006).

The reaction of NMP with a coal sample using the ASE instrument results in a brown liquid, with the consistency of syrup. This phenomenon can be attributed to the physical and chemical processes occurring within the cell as NMP reacts with the coal sample: the addition of the solvent causes the coal structure to swell causing bonds within the coal matrix to break. As a result, the addition of NMP caused the extraction cell to overflow in all experimental attempts. The liquid collected from the ASE extraction was then ashed, leached with HCl, evaporated to dryness and brought up in 2% HNO_3 for ICP analysis to determine the Fe content. The iron values reflect the presence of iron compounds not associated with the coal surface or a crystalline mineral phase. These findings confirm experimental data collected by Renganathan and Zondlo (Renganathan and Zondlo, 1993). The authors discovered that a small percentage of Fe remained in the NMP solution as $FeSO_4$ regardless of the experimental parameters used

(Zondlo, personal communication). The presence of iron within the liquid suggests the presence of C-Fe bonds which, when broken, react with sulfur produced from the breaking of C-S bonds.

Furthermore, the small amount of iron extracted by NMP is consistent with results presented by Narwall and Singh (Narwall and Singh, 2001). They conducted a study to investigate the solubility of iron and manganese and their association with soil components in soils. Data from their study indicated that only small fractions of total iron and manganese were associated with organic matter.

Although iron yield was 100% when the coal sample was extracted using EDTA and NMP, this does not necessarily imply that all iron within the sample was either bound to the surface or organically within the coal structure. First, exhaustive extractions were undertaken during the EDTA step to ensure that surficial iron species were extracted during the first extraction step. The significant decrease in the amount of iron extracted between the first EDTA extraction step and the last (72.46% → 15.92%) may indicate that, due to the presence of excess EDTA, crystalline iron-bearing phases were attacked during the second and third extraction (Raiswell et al., 1994). If only the iron yield from the first EDTA extraction (EDTA 1) is considered, then the amount of iron extracted using the EDTA, followed by NMP, is approximately 80% (**Table 15**). This implies that approximately 20% of the remaining iron within the sample is contained in mineral phases; however, the calculated mineral matter content (**Table 11**) for sample CL-TC-CL1, based on iron concentrations determined from HCl leaches of ash, is only 9%. This discrepancy could be attributed to a) variations in iron content within samples; b) a non-optimal combination of experimental parameters (**Table 17**) used for ASE extractions; or c) the measured iron content of leached high temperature ash (HTA) samples not reflecting a sample's total iron concentration. With respect to the latter, ferrous compounds are

typically oxidized during the HTA procedures and Fe^{3+} compounds fully dissolve in reducing acids such as HCl. However, HCl is not en effective reagent to dissolve iron remaining bound to sulfides, or within silicates; an oxidizing acid is needed. For example, the decomposition of pyrite to pyrrhotite, followed by oxididation from the surface inward to produce molten FeO-FeS phases, does not occur below a temperature of 1080°C (McLennan et al., 2000), far exceeding the ashing temperature used in this study. Therefore, without an additional chemical extraction, the iron leached from the ash represents only HCl- soluble iron and is not an accurate representation of the entire iron reservoir within the sample. To ensure that all iron is leached from ash samples, the samples should be leached with either HNO_3 and/or HF (after leaching with HCl) to solubilize any sulfide- or silicate-bound iron.

To date, no studies using NMP to extract organic matter using an ASE instrument, or to understand iron associations within the coal structure, have been reported. Additional research is needed to optimize extraction parameters for this novel method.

4.4.2 *Chemical Extractions*

A comprehensive review of reagents and extraction schemes are provided by (Gleyzes et al., 2002) and references therein. The method used below loosely followed the procedure presented by Lord (1980) and Poulton and Canfield (2005). This particular sequence of reagents was selected to a) minimize oxidation of pyrite during the extraction procedure yet b) quantitatively extract iron bound to carbonate and oxide phases.

4.4.2.1 *Siderite*

Sodium acetate, buffered with acetic acid to pH = 5, is commonly used to extract carbonates from sediment (Gleyzes et al., 2002; Rao et al., 2008; Sahuquillo et al., 2003). Poulton and Canfield (2005) determined the optimum extraction times using different reagents for iron carbonates and oxides and concluded that for sediments where crystalline siderite is not a significant sample component, a 24-h, room temperature acetate extraction at pH 4.5 is sufficient for the complete dissolution of ankerite ($Ca(Fe, Mg, Mn)(CO_3)_2$), poorly crystalline $FeCO_3$, and for the determination of trace Fe associated with carbonate phases. Iron yield for synthetic siderite dissolved using these parameters was 100%; however, the yield dropped considerably when natural samples of siderite were analyzed (**Table 17**).

Table 17. A comparison of different experimental parameters used to extract iron (in wt%) from iron carbonates using sodium acetate, buffered to the desired pH with acetic acid. Data shown for samples 1-3 are from Poulton and Canfield (2005). Sample 4 is data collected during this study.

Mineral	Total Fe	pH 4, 24h		pH 4.5, 24h		pH 5, 24h		pH 4.5, 48h, 50°C	
	mg/g	*mg/g*	*% Yield*	*mg/g*	*% Yield*	*mg/g*	*% Yield*	*mg/g*	*% Yield*
1 - $FeCO_3$, syn	46.2	46.1	99.8	46.2	100	32.8	71.0	46.1	99.8
2 - Roxbury Sid	28.9	24.8	85.8	24.4	84.4	22.4	77.5	28.1	97.2
3 - Biwabik Sid	22.3	14.5	65.0	12.3	55.2	4.1	18.4	21.3	95.2
4 – Kossuth Sid	51.4	17.6	34.4	—		—		—	

The difference in iron yield for natural siderite samples is complicated by the fact that natural siderite rarely occurs in pure form. For example, XRD analyses of the Roxbury siderite sample (#2) revealed the presence of hematite, and a significant proportion of stilpnomelane, an iron rich sheet silicate, was found in the Biwabik (#3) sample (Poulton and Canfield, 2005). No

analyses were conducted to elucidate the purity of the Kossuth siderite sample (#4), however, the surface of the siderite nodules indicated the presence of oxidation products. Furthermore, nodules collected from this area contain high concentrations of silicate minerals.

The anomalously high iron yield from siderite in the unspiked samples (DECS 24A and DECS 24B; see **Table 16**) can be attributed to parallel dissolution of pyrite and siderite over the experimental time period. Documentation provided with this sample (PSU Coal Database) indicated that the pyrite content was about 5% in sample DECS-24.

4.4.2.2 *Iron Oxides: Goethite*

A primary problem in devising extraction schemes for transition metals is selecting agents that are effective in solubilizing a given form of the element and relatively selective for that particular form (Narwall and Singh, 2001). Chemical phases within sediment can also be influenced by the experimental conditions and labile fractions can be transformed during sample preparation and during sequential extractions.

Although sodium dithionite has been successfully used to dissolve crystalline iron oxides in previous studies (Gleyzes et al., 2002; Rao et al., 2008; Sahuquillo et al., 2003), the iron yield from both the synthetic, spiked and mixed mineral samples were <1%. This is surprising: visual observations of the test tubes containing only goethite revealed that the mineral had completely dissolved and no residue was collected following this step. Subsequent to analysis, samples were inspected to determine if solids had precipitated out of solution thus causing the apparent low iron yield. Visual inspection revealed no precipitation. Roychoudbury (Roychoudhury, 2006) reports anomalous dissolution behavior of crystalline oxides, such as goethite, depending on the amount of organic matter present; the presence of organic matter may enhance recovery of

metals or reduce the time it takes to dissolve a chemical phase. While the iron yield was greater for the ash sample spiked with goethite, overall recovery was less than 1%.

Adsorption and redistribution of metals among different phases during extraction seems to influence the majority of results in single step and sequential extraction schemes. Roychoudbury (Roychoudhury, 2006) reports that up to 100% readsorption of trace metals onto the sediments has been observed regardless of the strength of the reagent used. It is possible that samples containing coal ash, spiked with known amounts of iron minerals, acted as a sorbent surface for the reagents and dissolved iron. Due to the high surface site density of coal, active exchange of iron in the solid and aqueous phases with the coal surface may have resulted in low iron yield for samples containing goethite. Nonetheless, the causes of this apparent discrepancy between visual observation and analytical analysis remains unclear.

4.4.2.3 *Pyrite*

Concentrated nitric acid was used to dissolve pyrite and the results are similar to those collected for goethite: the analyzed iron yield was very low. No residue remained in the test tubes containing only pyrite and, based on a visual inspection of the samples at the conclusion of this step, the reagent was successful in dissolving pyrite. Again, the cause of this discrepancy has not been resolved.

4.5 CONCLUSIONS

Initial results from accelerated solvent extraction (ASE) leaching experiments indicate that the majority of iron within coal samples is either bound to the surface of the coal or located

within the macromolecular coal structure (organically bound) instead of within solid crystalline phases, such as pyrite. However, further work is required to assess the extent to which coal mineral matter such as pyrite may have been solubilized by EDTA and NMP at relatively high temperatures and pressures.

Spiking experiments, utilized in this study, provide valuable information regarding the selectivity and efficiency of a proposed sequential extraction technique for geologic samples. Thermodynamic modeling of these reactions using geochemical software could provide additional insight into trace element behavior during sequential leaching. No theoretical studies have been published, to the author's knowledge, that simulate plausible chemical reactions/elemental speciation that occur during individual leaching and sequential leaching using different reagents and experimental parameters (temperature, pH, etc.). The results presented above suggest that the developed sequential extraction scheme could be successfully used (in full or in part) to assess Fe partitioning in organic rich sediments such as coal; however, the discrepancy between measured iron values in iron oxides and pyrite samples and visual observations (apparent complete dissolution) must be resolved.

No sequential extraction methods have been published, to the author's knowledge, to assess metal distribution among various sedimentary phases within organic-rich sediments. However, extractions of sediments using the same reagents used in this study have reported 100% yield for target phases (Poulton and Canfield, 2005). Given the reported reproducibility of these reagents (Baeyens et al., 2003a; Filgueiras et al., 2002; Poulton and Canfield, 2005), the low recovery of iron from leached mineral samples within this study could be a result of analytical issues.

Sequential extraction experiments have been shown to provide a convenient means to determine the metals associated with the principal accumulative phases in sedimentary deposits (Filgueiras et al., 2002); however quantitative recovery can be affected by the sequence of extraction steps (Baeyens et al., 2003b; Narwall and Singh, 2001), sample type (Filgueiras et al., 2002; Kheboian and Bauer, 1987; Santamaria-Fernández et al., 2006), or experimental parameters such as reagent concentration, pH, etc (Rao et al., 2008; Shiowatana et al., 2001). I suggest that future studies employing geochemical modeling of reactions using different reagent and experimental parameters would not only provide insight into trace element behavior and speciation but be cost effective as well. Results would help establish a baseline on which to conduct experimental work, and comparisons between theoretical and experimental work could be analyzed and interpreted.

5.0 CONCLUSIONS

5.1 SUMMARY

The focus of this research was to investigate the geochemistry and iron isotope systematics of pyrite from hydrothermal and coal-forming environments. Analyses of changes that occur during oxidative pyrite dissolution improves our understanding of iron movement within Fe-bearing outflows, and provides insight into the biogeochemistry of this element, reaction mechanisms, and processes that occur in solid-liquid systems. In this study, iron isotopes were used to study dissolution rates of different pyrite types (hydrothermal versus sedimentary), and the relationship between sedimentary pyrite dissolution and the geochemical evolution of water was examined. Specific objectives included: 1) develop methods isolate pyrite and other iron-bearing phases for experimental analysis, with the goal of creating reproducible experimental results; 2) determine the $^{56}Fe/^{54}Fe$ variation of hydrothermal pyrite and sedimentary pyrite deposited under different environmental conditions; 3) establish if abiotic pyrite dissolution causes measurable shifts in the $^{56}Fe/^{54}Fe$ ratio of iron released into solution during batch reactor dissolution experiments; and 4) assess the efficacy of pyrite as a geochemical tracer for the primary source of iron in contaminated outflows.

In pyrite dissolution and oxidation experiments, massive hydrothermal pyrite is normally used because it is readily available and well characterized. However, sedimentary pyrite exists in

many forms, and pyrite mineral preparation methodologies are inconsistent within the literature. In the first stage of this investigation, dry and wet sieving methodologies for preparing pyrite for dissolution experiments were evaluated, and an effective, reproducible procedure was developed to isolate pyrite grains in the 44-75 micron (μm) range for pyrite dissolution studies (Wolfe et al., 2007).

Conventional batch reactor dissolution experiments were used to study the relative rates of dissolution of five sedimentary and three hydrothermal pyrite samples from different geologic origins. In the second phase of this study, pyrite prepared using the above methods was used in oxidative dissolution experiments (Liu et al., 2008a,b), and iron isotope ratios were measured in selected starting materials and dissolution products. Bulk pyrite δ^{56}Fe values range from -0.1 to +1.34, with hydrothermal bulk pyrite $\delta^{56}Fe < 0.5$ and coal and sedimentary pyrite nodule $\delta^{56}Fe \geq 0.5$. The hydrothermal pyrite falls within the range of previously measured values, but the coal/sedimentary values are higher than those previously measured for any Phanerozoic sedimentary pyrite. Aliquots of leachate samples from each pyrite dissolution experiment (pH=3) were collected for iron isotope analysis at 1, 8 and 24 hours from the start of the experiment. Iron was collected from leachate solutions using anion resin chromatography, and analyzed for $^{56}Fe/^{54}Fe$ ratios using MC-ICP-MS. Results from these data indicate that leachates from oxidative dissolution of the pyrite tend, with minor exceptions, to yield δ^{56}Fe values equal to or below those of the coexisting bulk pyrite, by up to ~1‰. This direction of fractionation is consistent with theoretical calculations; however, the shifts are not consistent in magnitude.

In order to effectively assess the mobility, availability, and contaminant risk of metals within any given geologic setting impacted by AMD, analytical methods are required not only to determine the total amount of each metal, but also the distribution of phases. Development of a

successful iron fractionation technique must take into account the dynamics of dissolution processes and their inhibition, and requires an appreciation of the reactions which describe the transfer of the chemical species between a given mineral, as well as an understanding of the structure and chemical bonding at the mineral-solution interface. In the third part of this study, a sequential extraction technique was developed to understand how iron is distributed in coal environments. Six sediment iron fractions were characterized: (1) surficially bonded Fe; (2) organically bound Fe (Fe_{org}); (3) carbonate-associated Fe; (4) reducible oxides; (5) silicate Fe; and (6) pyrite Fe. Iron fractions were determined using a combination of pressurized fluid extraction and chemical leaching on bituminous coal samples.

5.2 MAJOR CONCLUSIONS

The original contributions of this research include: 1) a sample preparation technique to isolate minerals within a specific size range for use in experimental dissolution studies; 2) analysis of iron isotope signatures within hydrothermal and sedimentary pyrite of varying petrogenetic history; 3) iron isotope analysis of experimental pyrite dissolution leachates; 4) development of a sequential extraction method to quantify and understand the physico-chemical distribution of iron within organic rich sediments such as coal.

The major conclusions reached by this work are presented below.

Sample preparation methods not only affect the pyrite size distribution, but also apparent dissolution rates. Data presented in Chapter 2, "*A method for generating uniform size-segregated pyrite particle fractions*" demonstrate that samples that are prepared using dry sieving techniques

exhibit far higher absolute dissolution rates than those prepared by wet sieving, due to the presence of fine particles that adhere to the particle surface. A wet sieving procedure was developed using vacuum filtration techniques to obtain fine (<100 μm) particle size fractions of pyrite for use in geochemical experiments. This method uses readily available materials and equipment, and has potential application to minerals other than pyrite. Only dissolution data from pyrite samples prepared using the same procedure and yielding the same particle size distribution and particle surface can be compared. This is essential for our ability to compare experimental results collected by other researchers.

In order to effectively address issues associated with the presence of Fe-enriched water from abandoned coal and metal mines, the processes and mechanisms governing pyrite dissolution and the subsequent geochemical evolution of water need to be understood. The application of iron isotopes could provide insight into pyrite oxidation processes, as well as provide a means for tracking the origin of iron in AMD-affected streams. Most experimental studies of pyrite dissolution have been conducted with hydrothermal pyrite. Results obtained from iron isotope analyses of experimental abiotic pyrite dissolution experiments (Chapter 3) show that bulk pyrite δ^{56}Fe values differ between hydrothermal and sedimentary pyrite samples. Hydrothermal pyrite samples fall within the range of previously measured values, but the coal/sedimentary values are higher than those previously measured for any Phanerozoic sedimentary pyrite. Leachates from oxidative dissolution of the pyrite at pH=3 tend, with minor exceptions, to yield δ^{56}Fe values equal to or below those of the coexisting bulk pyrite, by up to ~1‰. The δ^{56}Fe values of the pyrite leachates decrease with time. The direction of fractionation is consistent with theoretical calculations but the shifts are not consistent in magnitude. We conclude that iron isotope analyses have the capability to provide important information about surface processes during

oxidative dissolution of sulfides, and distinguishing between waters that interact with continentally-derived pyrite (e.g., from coal) and pyrite formed under marine conditions. Although the δ^{56}Fe of the leachates were not always equivalent to bulk pyrite values, the spread in bulk values is likely to allow differentiation of iron from these sources.

The development of a sequential extraction technique that targets specific "model" iron compounds known to occur in coal and combinations of compounds will confirm and provide more knowledge about the chemical mechanisms of pyrite formation, subsequent dissolution, and generation of AMD, as well as the extent to which the coal matrix affects mineral dissolution. An extraction technique to quantify and understand the physico-chemical distribution of iron within organic rich sediments, such as coal, was developed. Initial results suggest that much of the iron within coal samples could be either bound to the surface of the coal or within the macromolecular coal structure (organically bound) instead of within solid crystalline phases, such as pyrite. Alternatively, for extractions that take place under relatively high-pressure conditions, pyrite may be significantly leached by reagents commonly thought to attack only organic compounds. These results indicate that great care must be taken when chemically extracting iron from organic-rich sediments, and in operationally defining the Fe reservoirs in these samples.

5.3 RECOMMENDATIONS FOR FUTURE RESEARCH

The research presented in this dissertation suggests the following directions for further investigation:

- Results from this study indicate that differences may exist between syngenetic and epigenetic pyrite in coal seams. Trace element analyses, SEM analysis of morphology, and measurement of Fe isotope ratios of pyrite from coal seams, the coal seam underclay, and coal overburden would provide additional data to help constrain geochemical processes occurring during pyrite formation.

- Due to the lack of experimental isotope data of pyrite chemistry, it is difficult to interpret iron isotope signatures collected in natural environments. Iron isotope analyses collected during pyrite synthesis experiments, simulating low temperature conditions, would provide a much needed dataset regarding iron isotope signatures and fractionation associated with pyrite formation. In addition, a combined geochemical and iron isotope approach to pyrite synthesis experiments involving iron interactions with organic acids would more accurately reflect conditions where pyrite is formed. An investigation of iron isotope fractionation associated with 1) iron oxide dissolution in organic acids, and 2) pyrite formation generated from Fe(II) solutions produced through these organic–iron interactions would contribute a novel dataset and provide important insight into metallo-organic interactions and pyrite formation.

- To constrain iron isotope interpretations of AMD samples collected in the field, experimental simulations of AMD formation, using column experiments, are needed. In

such experiments, coal would be exposed to different leachant solutions of varying pH, and $^{56}Fe/^{54}Fe$ ratios would be measured for solutions collected at time intervals. These data would provide insight into processes occurring as pyrite dissolves and assist in identifying possible fractionation effects due to the dissolution process.

- Existing models of pyrite dissolution and AMD generation can be refined by coupling geochemical and iron isotope data collected from experimental simulations of AMD generation to iron isotope signatures of AMD outflow waters emanating from coal-bearing strata and the resulting precipitates. These data would help establish the relationship between reactive pyrite and iron within outflow waters in AMD systems.

- The ability to quantitatively partition iron in coal and organic-rich sediments would not only aid in our understanding of AMD generation, but could also provide important information about iron biogeochemistry and the petrogenesis of Fe-rich phases such as pyrite in modern and ancient sedimentary environments. Isotope analyses of iron collected from the different fractions may present isotopic end members which could in turn be used identify sources of iron and/or track mechanisms for the formation of pyrite. Consequently, the sequential extraction technique presented in this research for identification of iron phases within coal should be optimized so that the method is applicable to numerous organic samples, with good reproducibility.

REFERENCES

Anbar, A.D., Roe, J.E., Barling, J., and Nealson, K.H., 2000, Nonbiological fractionation of iron isotopes: Science, v. 288, p. 126-128.

Archer, C., and Vance, D., 2006, Coupled Fe and S isotope evidence for Archean microbial Fe(III) and sulfate reduction: Geology, v. 34, p. 153-156.

Arnold, G.L., Weyer, S., and Anbar, A.D., 2004, Fe isotope variations in natural materials measured using high mass resolution multiple collector ICPMS: Analytical Chemistry, v. 76, p. 322-327.

Assis, L.M., Sebastião Silva Pinto, J., and Mauro Lanças, F., 2000, Comparison among different extraction methods (PFE, SFE, Sonication, Soxhlet) for the isolation of organic compounds from coal: Journal of Microcolumn Separations, v. 12, p. 292-301.

Badin, E.J., 1984, Coal Combustion Chemistry - Correlations Aspects: New York, Elsevier.

Baeyens, W., Monteny, F., Leermakers, M., and Bouillon, S., 2003a, Evaluation of sequential extractions on dry and wet sediments: Analytical and Bioanalytical Chemistry, v. 376, p. 890-901.

Bassi, R., Prasher, S.O., and Simpson, B., 2000, Extraction of metals from a contaminated sandy soil using citric acid: Environmental Progress, v. 19, p. 275-282.

Beard, B.L., and Johnson, C.M., 1999, High precision iron isotope measurements of terrestrial and lunar materials: Geochimica Et Cosmochimica Acta, v. 63, p. 1653-1660.

Bergquist, B.A., and Boyle, E.A., 2006, Iron isotopes in the Amazon River system: Weathering and transport signatures: Earth and Planetary Science Letters, v. 248, p. 54-68.

Berner, R.A., 1984, Sedimentary pyrite formation: an update: Geochimica Et Cosmochimica Acta, v. 48, p. 605 - 615.

Bonnissel-Gissinger, P., Alnot, M., Ehrhardt, J.-J., and Behra, P., 1998, Surface Oxidation of Pyrite as a Function of pH: Environmental Science & Technology, v. 32, p. 2839-2845.

Borek Sandra, L., 1993, Effect of Humidity on Pyrite Oxidation, Environmental Geochemistry of Sulfide Oxidation, Volume 550: ACS Symposium Series, American Chemical Society, p. 31-44.

Borrok, D.M., Nimick, D.A., Wanty, R.B., and Ridley, W.I., 2008, Isotopic variations of dissolved copper and zinc in stream waters affected by historical mining: Geochimica Et Cosmochimica Acta, v. 72, p. 329-344.

Borrok, D.M., Wanty, R.B., Ridley, W.I., Lamothe, P.J., Kimball, B.A., Verplanck, P.L., and Runkel, R.L., 2009, Application of iron and zinc isotopes to track the sources and mechanisms of metal loading in a mountain watershed: Applied Geochemistry, v. 24, p. 1270-1277.

Brantley, S.L., Liermann, L., and Bullen, T.D., 2001, Fractionation of Fe isotopes by soil microbes and organic acids: Geology, v. 29, p. 535-538.

Bullen, T.D., White, A.F., Childs, C.W., Vivit, D.V., and Schulz, M.S., 2001, Demonstration of significant abiotic iron isotope fractionation in nature: Geology, v. 29, p. 699-702.

Butler, I.B., Archer, C., Vance, D., Oldroyd, A., and Rickard, D., 2005, Fe isotope fractionation on FeS formation in ambient aqueous solution: Earth and Planetary Science Letters, v. 236, p. 430-442.

Caldeira, C.L., Ciminelli, V.S.T., Dias, A., and Osseo-Asare, K., 2003, Pyrite oxidation in alkaline solutions: nature of the product layer: International Journal of Mineral Processing, v. 72, p. 373-386.

Canfield, D., 1989, Reactive iron in marine sediments: Geochimica Et Cosmochimica Acta, v. 53, p. 619-632.

Canfield, D.E., Raiswell, R., and Bottrell, S., 1992, The reactivity of sedimentary iron minerals toward sulfide: American Journal of Science, v. 292, p. 659-683.

Cruz, R., Bertrand, V., Monroy, M., and González, I., 2001, Effect of sulfide impurities on the reactivity of pyrite and pyritic concentrates: a multi-tool approach: Applied Geochemistry, v. 16, p. 803-819.

Descostes, M., Vitorge, P., and Beaucaire, C., 2004, Pyrite dissolution in acidic media: Geochimica Et Cosmochimica Acta, v. 68, p. 4559-4569.

Domagal-Goldman, S.D., and Kubicki, J.D., 2008, Density functional theory predictions of equilibrium isotope fractionation of iron due to redox changes and organic complexation: Geochimica Et Cosmochimica Acta, v. 72, p. 5201-5216.

Duan, Y., Severmann, S., Anbar, A.D., Lyons, T.W., Gordon, G.W., and Sageman, B.B., 2010, Isotopic evidence for Fe cycling and repartitioning in ancient oxygen-deficient settings:

Examples from black shales of the mid-to-late Devonian Appalachian basin: Earth and Planetary Science Letters, v. 290, p. 244-253.

Emmanuel, S., Erel, Y., Matthews, A., and Teutsch, N., 2005, A preliminary mixing model for Fe isotopes in soils: Chemical Geology, v. 222, p. 23-34.

Evangelou, V.P., 1995, Pyrite Oxidation and its Control: Boca Raton, CRC Press.

Fantle, M.S., and DePaolo, D.J., 2004, Iron isotopic fractionation during continental weathering: Earth and Planetary Science Letters, v. 228, p. 547-562.

—, 2005, Variations in the marine Ca cycle over the past 20 million years: Earth and Planetary Science Letters, v. 237, p. 102-117.

Fehr, M.A., Andersson, P.S., Halenius, U., Gustafsson, O., and Morth, C.M., 2010, Iron enrichments and Fe isotopic compositions of surface sediments from the Gotland Deep, Baltic Sea: Chemical Geology, v. 277, p. 310-322.

Fernandez, A., and Borrok, D.M., 2009, Fractionation of Cu, Fe, and Zn isotopes during the oxidative weathering of sulfide-rich rocks: Chemical Geology, v. 264, p. 1-12.

Filgueiras, A.V., Lavilla, I., and Bendicho, C., 2002, Chemical sequential extraction for metal partitioning in environmental solid samples: Journal of Environmental Monitoring, v. 4, p. 823-857.

Gleyzes, C., Tellier, S., and Astruc, M., 2002, Fractionation studies of trace elements in contaminated soils and sediments: a review of sequential extraction procedure: TrAC Trends in Analytical Chemistry, v. 21, p. 451-467.

Graham, S., Pearson, N., Jackson, S., Griffin, W., and O'Reilly, S.Y., 2004, Tracing Cu and Fe from source to porphyry: in situ determination of Cu and Fe isotope ratios in sulfides from the Grasberg Cu-Au deposit: Chemical Geology, v. 207, p. 147-169.

Graham, U.M., and Ohmoto, H., 1994, Experimental-study of formation mechanisms of hydrothermal pyrite: Geochimica et Cosmochimica Acta, v. 58, p. 2187-2202.

Hammack RW, L.R., and Diehl JR, 1988, Methods for determining fundamental chemical differences between iron disulfides from different geologic environments, U.S. Bureau of Mines Information Circular 9183, U.S. Bureau of Mines Information

Herbert, R.B., and Schippers, A., 2008, Iron isotope fractionation by biogeochemical processes in mine tailings: Environmental Science & Technology, v. 42, p. 1117-1122.

Huerta-Diaz, M.A., and Morse, J.W., 1990, A quantitative method for determination of trace metal concentrations in sedimentary pyrite: Marine Chemistry, v. 29, p. 119-144.

Ingri, J., Malinovsky, D., Rodushkin, I., Baxter, D.C., Widerlund, A., Andersson, P., Gustafsson, O., Forsling, W., and Ohlander, B., 2006, Iron isotope fractionation in river colloidal matter: Earth and Planetary Science Letters, v. 245, p. 792-798.

Jerz, J.K., and Rimstidt, J.D., 2004, Pyrite oxidation in moist air: Geochimica et Cosmochimica Acta, v. 68, p. 701-714.

Jiann, K.-T., and Presley, B.J., 2002, Preservation and Determination of Trace Metal Partitioning in River Water by a Two-Column Ion Exchange Method: Analytical Chemistry, v. 74, p. 4716-4724.

Johnson, C.M., and Beard, B.L., 1999, Correction of instrumentally produced mass fractionation during isotopic analysis of Fe by thermal ionization mass spectrometry: International Journal of Mass Spectrometry, v. 193, p. 87-99.

Kamei, G., and Ohmoto, H., 2000, The kinetics of reactions between pyrite and O-2-bearing water revealed from in situ monitoring of DO, Eh and pH in a closed system: Geochimica et Cosmochimica Acta, v. 64, p. 2585-2601.

Kheboian, C., and Bauer, C., 1987, Accuracy of Selective Extraction Procedure for Metal Speciation in Model Aquatic Sediments: Analytical Chemistry, v. 59, p. 1417 - 1423.

Kirpichtchikova, T.A., Manceau, A., Spadini, L., Panfili, F., Marcus, M.A., and Jacquet, T., 2006, Speciation and solubility of heavy metals in contaminated soil using X-ray microfluorescence, EXAFS spectroscopy, chemical extraction, and thermodynamic modeling: Geochimica et Cosmochimica Acta, v. 70, p. 2163-2190.

Kortenski, J., and Kostova, I., 1996, Occurrence and morphology of pyrite in Bulgarian coals: International Journal of Coal Geology, v. 29, p. 273-290.

Li, X., Coles, B.J., Ramsey, M.H., and Thornton, I., 1995, Sequential extraction of soils for multielement analysis by ICP-AES: Chemical Geology, v. 124, p. 109-123.

Liu, R., 2006, Electrochemical Study of Pyrite Dissolution: Pittsburgh, Carnegie Mellon University

Liu, R., Wolfe, A.L., Dzombak, D.A., Stewart, B.W., and Capo, R.C., 2008, Comparison of dissolution under oxic acid drainage conditions for eight sedimentary and hydrothermal pyrite samples: Environmental Geology, v. 56, p. 171-182.

Lord, C.J., 1982, A selective and precise method for pyrite determination in sedimentary materials: Journal of Sedimentary Research, v. 52, p. 664-666.

Lowson, R.T., 1982, Aqueous oxidation of pyrite by molecular oxygen: Chemical Reviews, v. 82, p. 461-497.

Marechal, C.N., Telouk, P., and Albarede, F., 1999, Precise analysis of copper and zinc isotopic compositions by plasma-source mass spectrometry: Chemical Geology, v. 156, p. 251-273.

Matthews, A., Morgans-Bell, H.S., Emmanuel, S., Jenkyns, H.C., Erel, Y., and Halicz, L., 2004, Controls on iron-isotope fractionation in organic-rich sediments (Kimmeridge Clay, Upper Jurassic, southern England): Geochimica Et Cosmochimica Acta, v. 68, p. 3107-3123.

McGuire, M.M., Edwards, K.J., Banfield, J.F., and Hamers, R.J., 2001, Kinetics, surface chemistry, and structural evolution of microbially mediated sulfide mineral dissolution: Geochimica et Cosmochimica Acta, v. 65, p. 1243-1258.

McKibben, M.A., and Barnes, H.L., 1986, Oxidation of pyrite in low temperature acidic solutions: Rate laws and surface textures: Geochimica et Cosmochimica Acta, v. 50, p. 1509-1520.

McLennan, A.R., Bryant, G.W., Bailey, C.W., Stanmore, B.R., and Wall, T.F., 2000, An Experimental Comparison of the ASh Formed from Coals Containing Pyrite and Siderite Mineral in Oxidizing and Reducing Conditions: Energy & Fuels, v. 14, p. 308-315.

Moses, C.O., Nordstrom, D.K., Herman, J.S., and Mills, A.L., 1987, Aqueous pyrite oxidation by dissolved-oxygen and by ferric iron: Geochimica et Cosmochimica Acta, v. 51, p. 1561-1571.

Murowchick, J.B., and Barnes, H.L., 1987, Effects of temperature and degree of supersaturation on pyrite morphology: American Mineralogist, v. 72, p. 1241-1250.

Narwall, R.P., and Singh, B.R., 2001, Solid Phase Speciation of Iron and Manganese in Alum Shale Soils Studied by Parallel and Sequential Extraction: Communications in Soil Science and Plant Analysis, v. 32, p. 331 - 349.

Nishizawa, M., Yamamoto, H., Ueno, Y., Tsuruoka, S., Shibuya, T., Sawaki, Y., Yamamoto, S., Kon, Y., Kitajima, K., Komiya, T., Maruyama, S., and Hirata, T., 2010, Grain-scale iron isotopic distribution of pyrite from Precambrian shallow marine carbonate revealed by a femtosecond laser ablation multicollector ICP-MS technique: Possible proxy for the redox state of ancient seawater: Geochimica Et Cosmochimica Acta, v. 74, p. 2760-2778.

Paschka, M.G., and Dzombak, D.A., 2004, Use of dissolved sulfur species to measure pyrite dissolution in water at pH 3 and 6: Environmental Engineering Science, v. 21, p. 411-420.

Polyakov, V.B., 1997, Equilibrium fractionation of the iron isotopes: Estimation from Mossbauer spectroscopy data: Geochimica Et Cosmochimica Acta, v. 61, p. 4213-4217.

Polyakov, V.B., and Mineev, S.D., 1999, Mossbauer spectroscopy as applied to isotopic geochemistry: I. Equilibrium fractionation of iron isotopes: Geokhimiya, p. 858-870.

Poulton, S.W., and Canfield, D.E., 2005, Development of a sequential extraction procedure for iron: implications for iron partitioning in continentally derived particulates: Chemical Geology, v. 214, p. 209-221.

Raiswell, R., Canfield, D.E., and Berner, R.A., 1994, A comparison of iron extraction methods for the determination of degree of pyritisation and the recognition of iron-limited pyrite formation: Chemical Geology, v. 111, p. 101-110.

Rao, C., Sahuquillo, A., and Lopez Sanchez, J., 2008, A Review of the Different Methods Applied in Environmental Geochemistry For Single and Sequential Extraction of Trace Elements in Soils and Related Materials: Water, Air, & Soil Pollution, v. 189, p. 291-333.

Rauret, G., 1998, Extraction procedures for the determination of heavy metals in contaminated soil and sediment: Talanta, v. 46, p. 449-455.

Renganathan, K., and Zondlo, J.W., 1993, Non-destructive extraction mechanism of bituminous coals using N-methyl-2-pyrrolidone: Fuel science & technology international, v. 11, p. 677-695

Rickard, D., and Luther, G.W., 2007, Chemistry of iron sulfides: Chemical Reviews, v. 107, p. 514-562.

Rigby, P.A., Dobos, S.K., Cook, F.J., and Goonetilleke, A., 2006, Role of organic matter in framboidal pyrite oxidation: Science of the Total Environment, v. 367, p. 847-854.

Rimstidt, J.D., and Vaughan, D.J., 2003, Pyrite oxidation: A state-of-the-art assessment of the reaction mechanism: Geochimica et Cosmochimica Acta, v. 67, p. 873-880.

Rouxel, O., Dobbek, N., Ludden, J., and Fouquet, Y., 2003, Iron isotope fractionation during oceanic crust alteration: Chemical Geology, v. 202, p. 155-182.

Rouxel, O., Fouquet, Y., and Ludden, J.N., 2004, Subsurface processes at the Lucky Strike hydrothermal field, Mid-Atlantic Ridge: Evidence from sulfur, selenium, and iron isotopes: Geochimica Et Cosmochimica Acta, v. 68, p. 2295-2311.

Rouxel, O.J., Bekker, A., and Edwards, K.J., 2005, Iron isotope constraints on the Archean and Paleoproterozoic ocean redox state: Science, v. 307, p. 1088-1091.

Roychoudhury, A.N., 2006, Time dependent calibration of a sediment extraction scheme: Marine Pollution Bulletin, v. 52, p. 397-403.

Sahuquillo, A., Rigol, A., and Rauret, G., 2003, Overview of the use of leaching/extraction tests for risk assessment of trace metals in contaminated soils and sediments: TrAC Trends in Analytical Chemistry, v. 22, p. 152-159.

Santamaria-Fernández, R., Cave, M.R., and Hill, S.J., 2006, Trace metal distribution in the Arosa estuary (N.W. Spain): The application of a recently developed sequential extraction procedure for metal partitioning: Analytica Chimica Acta, v. 557, p. 344-352.

Sasaki, K., 1994, Effect of grinding on the rate of oxidation of pyrite by oxygen in acid solutions: Geochimica et Cosmochimica Acta, v. 58, p. 4649-4655.

Schauble, E.A., Rossman, G.R., and Taylor, H.P., 2001, Theoretical estimates of equilibrium Fe-isotope fractionations from vibrational spectroscopy: Geochimica Et Cosmochimica Acta, v. 65, p. 2487-2497.

Schieber, J., 2002, Sedimentary pyrite: A window into the microbial past: Geology, v. 30, p. 531-534.

Severmann, S., Johnson, C.M., Beard, B.L., and McManus, J., 2006, The effect of early diagenesis on the Fe isotope compositions of porewaters and authigenic minerals in continental margin sediments: Geochimica Et Cosmochimica Acta, v. 70, p. 2006-2022.

Severmann, S., Lyons, T.W., Anbar, A., McManus, J., and Gordon, G., 2008, Modern iron isotope perspective on the benthic iron shuttle and the redox evolution of ancient oceans: Geology, v. 36, p. 487-490.

Sharma, M., Polizzotto, M., and Anbar, A.D., 2001, Iron isotopes in hot springs along the Juan de Fuca Ridge: Earth and Planetary Science Letters, v. 194, p. 39-51.

Shiowatana, J., Tantidanai, N., Nookabkaew, S., and Nacapricha, D., 2001, A Novel Continuous-Flow Sequential Extraction Procedure for Metal Speciation in Solids: J. Environ. Qual., v. 30, p. 1195-1205.

Steel, K.M., Besida, J., O'Donnell, T.A., and Wood, D.G., 2001, Production of Ultra Clean Coal: Part I--Dissolution behaviour of mineral matter in black coal toward hydrochloric and hydrofluoric acids: Fuel Processing Technology, v. 70, p. 171-192.

Stoffa, J.M., 2006, The Dissolution and Swelling of Bituminous Coal in N-Methyl-Pyrrolidone: Morgantown, West Virginia University.

Urey, H.C., 1947, The thermodynamic properties of isotopic substances: Chemical Society (London), p. 562 – 581.

Vassilev, S.V., and Vassileva, C.G., 1996, Occurrence, abundance and origin of minerals in coals and coal ashes: Fuel Processing Technology, v. 48, p. 85-106.

Ward, C.R., 2002, Analysis and significance of mineral matter in coal seams: International Journal of Coal Geology, v. 50, p. 135-168.

Weber, P.A., Stewart, W.A., Skinner, W.M., Weisener, C.G., Thomas, J.E., and Smart, R.S.C., 2004, Geochemical effects of oxidation products and framboidal pyrite oxidation in acid mine drainage prediction techniques: Applied Geochemistry, v. 19, p. 1953-1974.

Wiese, R.G., Jr. and Fyfe, W.S., 1986, Occurrences of iron sulfides in Ohio coals: International Journal of Coal Geology, v. 6, p. 251-276.

Wilkin, R.T., Barnes, H.L., and Brantley, S.L., 1996, The size distribution of framboidal pyrite in modern sediments: An indicator of redox conditions: Geochimica Et Cosmochimica Acta, v. 60, p. 3897-3912.

Williamson, M.A., and Rimstidt, J.D., 1994, The kinetics and electrochemical rate-determining step of aqueous pyrite oxidation: Geochimica et Cosmochimica Acta, v. 58, p. 5443-5454.

Wolfe, A.L., Liu, R., Stewart, B.W., Capo, R.C., and Dzombak, D.A., 2007, A method for generating uniform size-segregated pyrite particle fractions: Geochemical Transactions, v. 8, p. 1-8.

Yamaguchi, K.E., Johnson, C.M., Beard, B.L., Beukes, N.J., Gutzmer, J., and Ohmoto, H., 2007, Isotopic evidence for iron mobilization during Paleoproterozoic lateritization of the Hekpoort paleosol profile from Gaborone, Botswana: Earth and Planetary Science Letters, v. 256, p. 577-587.

Younger, P.L., Banwart, S.A., and Hedin, Robert S. , 2002, Mine Water: Hydrology, Pollution, Remediation: Boston, Kluwer Academic, p. 464 pages